

Bistable interstitial-carbon–substitutional-carbon pair in silicon

L. W. Song,* X. D. Zhan, B. W. Benson, and G. D. Watkins

Department of Physics and Sherman Fairchild Center for Solid State Studies, Lehigh University, Bethlehem, Pennsylvania 18015

(Received 23 January 1990)

A bistable interstitial-carbon–substitutional-carbon pair has been identified in electron-irradiated silicon by a combination of several spectroscopic experimental techniques. In the positive and negative charge states, the stable configuration of the defect involves a carbon-silicon “molecule” which occupies a single lattice site (each atom threefold coordinated) next to a substitutional-carbon atom (fourfold coordinated). In the neutral charge state, the defect rearranges its bonds so that both carbon atoms become substitutional (fourfold coordinated) with a twofold-coordinated silicon atom nestled between them. Detailed microscopic models and configurational-coordinate energy surfaces for each of the three charge states have been obtained.

I. INTRODUCTION

Defects in semiconductors that display metastable or bistable electronic properties are of great current interest.^{1,2} Examples include *DX* centers in $\text{Al}_x\text{Ga}_{1-x}\text{As}$ and $\text{GaAs}_{1-x}\text{P}_x$,³ *EL2* in GaAs ,⁴ *In* in CdF_2 ,⁵ the early thermal donors in silicon^{6,7} and germanium,⁸ and several radiation-produced and impurity-related defects in *InP* (Refs. 9 and 10) and silicon.^{11–24} Bistability can occur wherever the stable configuration of a defect in the lattice changes with its charge state and a barrier exists for conversion from one configuration to the other.^{1,2} In the particular case of Fe-acceptor pairs in silicon,^{11,12} a model has been proposed in which the change in Coulomb interaction between the relatively mobile interstitial Fe_i^{2+} or Fe_i^+ and the negatively charged substitutional acceptor causes a change in the relative stability of the nearest or next-nearest-neighbor position for Fe_i . This model has also been suggested^{1,25} to account for metastability effects recently reported for defects believed to be associated with interstitial C_i^- and C_i^{2-} paired with positively charged substitutional group-V donors.^{15–18,25} In no other case, however, is there a well-established picture of the mechanism nor in most cases even of the identity of the constituents of the defect involved.¹

In this paper we present a detailed experimental study of an important new bistable defect in electron-irradiated silicon. A series of experimental results involving deep-level capacitance transient spectroscopy (DLTS), electron paramagnetic resonance (EPR), and photoluminescence (PL) provide a clear and unambiguous identification of the defect as a carbon-interstitial–carbon-substitutional (C_iC_s) pair.^{19,20} We confirm, from the microscopic structural information, that a bistable level previously studied by DLTS in *n*-type material¹³ arises from the acceptor state of the C_iC_s pair. We find in addition that its donor state observed in *p*-type material also displays the same bistability. A new DLTS peak at $E_v + 0.09$ eV is detected associated with the C_iC_s donor state in the configuration stable when positively charged. From the PL experiments, we demonstrate that the well-known

0.97-eV luminescence (*G* line) (Refs. 26–28) arises from the same bistable C_iC_s defect and from the configuration stable for its neutral charge state only. All of the relevant energies for the configurational-coordinate surfaces of each of the three charge states are determined. We deduce detailed microscopic models for the two configurations and the mechanism for conversion between them.

This paper is organized as follows: Sec. II describes the experimental procedures and sample preparations in this study. A summary of the previous studies relevant to this work is given in Sec. III. These include a review of the bistable $E_c - 0.17$ eV defect reported in electron-irradiated *n*-type silicon¹³ and carbon-related defects studied by EPR, optical detection of magnetic resonance (ODMR), and infrared absorption (ir).

The details of the identification of the bistable nature of the C_iC_s pair are presented in Sec. IV. By presenting information gathered from several different experiments, a complete configurational-coordinate energy diagram is constructed. Finally, a microscopic model is deduced and the mechanism for the bistability of the defect is discussed in Sec. V. Some of the controversial arguments proposed in the earlier studies are also discussed and summarized.

II. EXPERIMENTAL DETAILS

A. Sample preparation

All silicon samples used in this study were floating-zone-grown (FZ) material with different dopants and impurity concentrations, as shown in Table I. The substitutional carbon concentration [*C*] was estimated for the *n*-type samples by measuring the intensity of the ir local-mode absorption band at 607 cm^{-1} at room temperature.^{29,30} The limit of detection for these measurements was $\sim 10^{16}\text{ cm}^{-3}$. The interstitial oxygen concentration [*O*] was measured for these samples from the intensity of the ir absorption band at $9\text{ }\mu\text{m}$ at room temperature.^{30,31} For all samples measured, $[\text{O}] \leq 2 \times 10^{16}\text{ cm}^{-3}$, the

TABLE I. Wafers (DLTS) and bulk (EPR and PL) samples used in this study. All materials were FZ grown with oxygen concentration below ir detection ($[O] \leq 2 \times 10^{16} \text{ cm}^{-3}$).

Wafers	Bulk	Dopant concentration (cm^{-3})	[C] (cm^{-3})
<i>n</i> type			
No. 0 ("Monex")		$n = [P] \sim 8 \times 10^{15}$	
No. 1 ("F3-114")	No. 1	$n = [P] \sim 6 \times 10^{15}$	2.4×10^{16}
No. 2 ("A127-27A")	No. 2	$n = [P] \sim 1.2 \times 10^{15}$	1×10^{17}
No. 3 ("A231-9A")	No. 3	$n = [P] \sim 9 \times 10^{15}$	$\leq 10^{16}$
	No. 4 ["SL-210 (NTD)"]	$n = [P] \sim 3 \times 10^{15}$ ($p = [B] \sim 1 \times 10^{15}$)	1×10^{17} (^{13}C 60%)
<i>p</i> type			
No. 5 ("A623-16B")	No. 5	$p = [B] \sim 2.4 \times 10^{15}$	
No. 7 ("MOW-B-3")		$p = [B] \sim 1.5 \times 10^{15}$	
No. 8 ("F3-149")	No. 8	$p = [Al] \sim 1 \times 10^{16}$	
	No. 9 ("F3-151")	$p = [Ga] \sim 5 \times 10^{15}$	
	No. 6 ("SL-210")	$p = [B] \sim 1 \times 10^{15}$	1×10^{17} (^{13}C 60%)

minimum concentration that could be detected.

The Monex material (sample No. 0) obtained from Monsanto was in wafer form. The [C] and [O] concentrations were not measured due to the thinness of these samples. Wafers from the remaining materials were sliced from each boule in regions adjacent to that from which the bulk EPR and PL samples were obtained in order that a reliable correlation between DLTS and EPR (and PL) experiments could be made.

To avoid excess oxygen incorporation, either Schottky-barrier or ion-implanted junctions were fabricated for the DLTS samples. For the Schottky-barrier contacts, aluminum was used for *n*-type wafers and chromium for *p* type. For the ion-implanted diodes, boron (from a BF_3 gaseous source) was implanted into *n*-type wafers to form $p^+ - n$ junctions, and phosphorus (PH_3 source) was implanted into *p*-type wafers to form $n^+ - p$ junctions. A range of ion-beam energies was used (50–120 keV) in order to achieve higher concentration (~ 100 times higher than the wafer dopant concentration) for the "+" region. The implanted junctions were subsequently annealed in a N_2 atmosphere for 30 min at 850°C to cure the lattice damage from the ion beam during the implantation. Two or three diodes were mounted on a single TO-5 header so that different biases could be applied to the diodes under identical annealing conditions. Plasma etch was applied to some of the diodes to produce mesa structural junctions for optical access from the side.

The EPR and PL samples are also listed in Table I. Although the oxygen concentrations were below detection ($\leq 2 \times 10^{16} \text{ cm}^{-3}$) in all samples, they may still be comparable with the dopant concentration in some cases. Therefore, the intensity of the oxygen-vacancy pair EPR signal (*A* center) (Refs. 32 and 33) produced by e^- irradiation is a reliable relative measure of this background oxygen content.

A ^{13}C -enriched *p*-type sample (sample No. 6, $[B] \sim 10^{15} \text{ cm}^{-3}$) was obtained from Brower at Sandia National Laboratories (Albuquerque, NM). Some of the material of sample No. 6 was converted to *n*-type (sample No. 4) us-

ing the neutron-transmutation-doping (NTD) technique by Farmer at the University of Missouri at Columbia. The final net donor concentration by a four-probe measurement was $\sim 2 \times 10^{15} \text{ cm}^{-3}$.

The EPR samples were cut from the appropriate boule in the form of a rectangular parallelepiped with a $\langle 110 \rangle$ axis parallel to the long dimension (2.5 mm \times 2.5 mm \times 15–20 mm, or 1.8 mm \times 1.8 mm \times 15–20 mm to receive double *in situ* uniaxial stress). They were polished subsequently with No. 600 emery paper and etched for about 1 min in CP_4 solution. The samples used for the EPR studies were also used for the PL experiments, as will be discussed in Sec. V. Equivalent neodymium-doped yttrium aluminum garnet (Nd:YAG) laser injection conditions were provided for both EPR and PL in order that a quantitative correlation between the two studies could be made.

All the irradiations were performed at room temperature with $\sim 2.5\text{-MeV}$ electrons from a 3 MeV van de Graaff accelerator. The DLTS samples were mounted on a 15 cm \times 15 cm \times 1.25 cm aluminum block behind an aluminum "beam scraper" plate of the same dimension which had a 5.6 mm-diameter hole in the center to define the radiation area. The current density was kept low ($\leq 2 \mu\text{A}/\text{cm}^2$) so that little overheating would occur during the irradiation. The sample was cooled by two air blowers. The typical dose was $(1.5\text{--}3) \times 10^{16} e^-/\text{cm}^2$ for the DLTS samples.

The sample holder for the EPR and PL samples was a similar size aluminum plate but with a water cooling jacket mounted on the back. The aperture size was defined by either a 2.54 cm diameter hole or a 2.54 cm \times 1.25 cm rectangular hole in an aluminum beam scraper in front of the samples. The radiation current density was kept at $\leq 2 \mu\text{A}/\text{cm}^2$. The irradiation dose was monitored by integrating the current collected from the sample plate. In the experiments, the appropriate radiation dose could also be determined by monitoring the EPR signals as a function of irradiation dose, as will be discussed in Secs. IV and V.

B. Experimental procedures

The DLTS apparatus used in this study is very similar to that described by Lang³⁴ with a double boxcar analyzer. All DLTS scans were performed with increasing temperature. The electrical level positions were determined in the conventional manner by combining scans with several different rate windows, with a $2kT$ correction factor to account for the combined temperature dependences of the free carrier thermal velocity and the density of conduction band states.³⁵ Capture cross sections were assumed to be temperature independent in the small temperature range studied. Minority carrier injection was supplied by applying forward bias to the $n^+ - p$ or $p^+ - n$ diodes with a current density at $\sim 2 \text{ A/cm}^2$. In some cases, optical injection was performed using a Nd:YAG laser (1.16 eV) in order to make a correlation with the EPR experiments. For these experiments, a fused quartz light pipe was used to guide the light onto a mesa structural diode, the injection dose being monitored by the diode photocurrent.

All of the EPR experiments were performed on a 14-GHz balanced bolometer spectrometer, the samples being placed in the center of a TE₀₁₁ microwave cavity located in a Janis Varitemp cryostat.³⁶ Generally, the carbon-related EPR spectra were observed in dispersion in the temperature range 15–30 K. Uniaxial stress was supplied by an air piston through a stainless steel stress rod. This rod could be replaced by a fused quartz light pipe so that Nd:YAG laser light could be introduced to the sample.

The Nd:YAG laser (1.16 eV, Sylvania 607) was also used as the excitation for the PL experiments. Luminescence was collected through a Pyrex window on an Air-Products cold finger Heli-tron cryostat. Excitation was from the side, guided by a fused-quartz light pipe. Using a room-temperature silicon filter, the dominant luminescence line in irradiated FZ silicon with zero-phonon transition at 0.97 eV (Refs. 26–28) was selected by a monochromator ($\frac{1}{4}$ m-focal-length, Jarrell-Ash) with a resolution of 12 nm and detected by a cooled Ge detector (Northcoast EO 817S).

III. SUMMARY OF PREVIOUS STUDIES

A. The bistable $E_c - 0.17 \text{ eV}$ defect

An interesting bistable defect in electron-irradiated n -type silicon was first reported by Jellison,¹³ based on isothermal capacitance transient measurements. By monitoring the transient associated with an energy level at $E_c - 0.17 \text{ eV}$, it was found that it could be converted to a faster transient corresponding to a level at $E_c - 0.11 \text{ eV}$ under special pulsing conditions. The maximum component of the faster transient response was found when the majority carrier pulse width was much smaller than some characteristic time constant τ_p (associated with the conversion from the $E_c - 0.11 \text{ eV}$ transient to the $E_c - 0.17 \text{ eV}$ transient), and the reverse bias time between pulses was much longer than another characteristic time constant, τ_r (associated with the return conversion from $E_c - 0.17 \text{ eV}$ to $E_c - 0.11 \text{ eV}$). These two characteristic

time constants were found to be thermally activated and given by¹³

$$\tau_r = 7.5 \times 10^{-13} \exp[(0.174 \text{ eV})/kT], \quad (1)$$

$$\tau_p = 7.3 \times 10^{-13} \exp[(0.145 \text{ eV})/kT]. \quad (2)$$

Not all of the transient at $E_c - 0.17 \text{ eV}$ could be converted to that at $E_c - 0.11 \text{ eV}$. It was concluded therefore that there were two defects contributing to the $E_c - 0.17 \text{ eV}$ transient, a convertible part and a nonconvertible part. The annealing behavior also distinguished the two parts of the transients at $E_c - 0.17 \text{ eV}$. The convertible part annealed at $\sim 300^\circ\text{C}$ and the nonconvertible part around 400°C , the latter being very close to the annealing temperature of the oxygen-vacancy pair.^{33,37}

Based on these observations, Jellison suggested that there were two different defects responsible for the $E_c - 0.17 \text{ eV}$ transient. The oxygen-vacancy pair for the nonconvertible part of the signal, and another defect (perhaps an impurity trapped by the O-V pair) giving rise to $E_c - 0.17 \text{ eV} \leftrightarrow E_c - 0.11 \text{ eV}$ intraconversion.¹³ He proposed then that the best candidate for this impurity was carbon, since (1) carbon was known to be present in concentrations of $\sim 10^{16} \text{ cm}^{-3}$ in the material and (2) carbon was believed to pair preferentially with oxygen after irradiation.^{38,39}

Later, follow-up studies were performed with the DLTS technique.^{11,14} Again it was found that in order to observe the DLTS peak at $E_c - 0.11 \text{ eV}$, the time between majority pulses had to be very long and the width of the majority pulse, short, in agreement with the observation of Jellison. However, no complementary loss of the $E_c - 0.17 \text{ eV}$ peak was observed, its amplitude appearing constant. This was explained as resulting from the fact that electron emission giving rise to the $E_c - 0.17 \text{ eV}$ DLTS peak occurs at a higher temperature than the $E_c - 0.11 \text{ eV}$ to $E_c - 0.17 \text{ eV}$ conversion temperature.¹⁴

A configurational-coordinate diagram was constructed as shown in Fig. 1 to explain the bistability.¹¹ The defect is stable in the A configuration when it is in its negative charge state, and stable in the B configuration when neutral. The two emissions observed at $E_c - 0.17 \text{ eV}$ and $E_c - 0.11 \text{ eV}$ are associated, respectively, with each of these two configurations. The thermal barrier for conversion from B^- to A^- was determined by Jellison [Eq. (2)] to be $\sim 0.15 \text{ eV}$, as shown, while the barrier for $A^- \rightarrow B^0$ was found to be $\sim 0.17 \text{ eV}$ [Eq. (1)], identical to the A^- emission.¹³ One possibility, therefore, was that the barrier for conversion from $A^0 \rightarrow B^0$ is $\leq 0.17 \text{ eV}$, so that the $A^- \rightarrow B^0$ conversion is limited by the $A^- \rightarrow A^0$ emission.

With this configurational-coordinate diagram, Chantre *et al.* attempted to describe the bistability as arising from two configurations of the O-V pair.¹¹ This assumption was supported to some degree by earlier EPR studies.⁴⁰ There it was found that an excited configuration of the O-V pair, (O-V)₁₀₀* produced by 20.4-K irradiation in n -type silicon, converted to the normal O-V pair at $\sim 45 \text{ K}$ with a similar kinetics as in Eq. (1), although no reverse process was reported in these earlier studies.⁴⁰

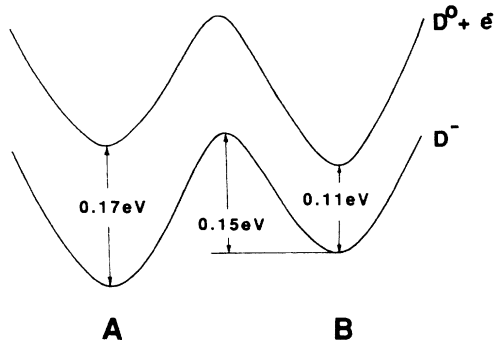


FIG. 1. Configurational-coordinate energy diagram proposed for the bistable $E_c - 0.17$ eV defect (Ref. 11). All three energy values were determined by Jellison (Ref. 13).

B. Carbon-related defects

Carbon is a common impurity in crystalline silicon. Substitutional carbon (C_s) may exceed a concentration of 10^{17} cm^{-3} in as-grown Czochralski (Cz) or FZ silicon and gives rise to an infrared localized vibrational mode²⁹ at 607 cm^{-1} . When such samples are irradiated with electrons below 300 K, mobile silicon interstitials (Si_i) and vacancies are produced and reactions between Si_i and C_s take place to produce isolated interstitial carbon (C_i).^{38,41} The C_i center has been studied extensively by local-mode absorption at 931 and 920 cm^{-1} [$C(1)$],³⁸ EPR [Si-G12],⁴¹ DLTS ($E_v + 0.28$ eV),^{42,43} and ir electronic absorption or luminescence at 856 meV.^{44,45} At $T \geq 300$ K, C_i atoms become mobile and have a tendency to complex with other impurities.

This scenario has been well established by EPR studies in p -type material: One of the dominant EPR centers produced by electron irradiation in the temperature range 100 – 300 K is the so-called Si-G12 spectrum.⁴¹ It was identified as arising from an isolated interstitial carbon in its donor charge state (C_i^+). Well-resolved ^{13}C hyperfine interactions and uniaxial stress coupling provided a microscopic model of the defect as a $\langle 100 \rangle$ C—Si interstitialcy which occupies a single substitutional site.

Coincident with the disappearance of the Si-G12 spectrum during 300 – 350 K isochronal annealing, another EPR spectrum, labeled Si-G11, was observed to emerge in FZ (low oxygen) p -type material.⁴⁶ With a ^{13}C -enriched sample, the spectrum split into two sets of well-resolved ^{13}C satellites indicating that two inequivalent carbon atoms are incorporated in the defect. The model proposed by Brower for Si-G11 was a $\langle 111 \rangle$ ($C_i C_s$)⁺ pair in which the two carbon atoms share a single lattice site. More recently, an optically detected magnetic resonance (ODMR) study showed that a luminescence band with zero-phonon line at 0.97 eV (G line) (Refs. 26 and 28) arises from exciton recombination at a neutral complex also involving two carbon atoms.^{47,48} The model deduced for this ODMR center consisted of two adjacent and equivalent substitutional carbon atoms with an interstitial silicon atom which has distorted out from a bond-

centered position between them.⁴⁸ The formation and annealing characteristics suggested that the 0.97 -eV luminescence and the Si-G11 EPR center arise from the same $C_i C_s$ defect but the different defect structural models deduced for the two argued against it.

In high-oxygen-content (Cz) material, on the other hand, oxygen can trap mobile C_i atoms. The resulting complex can be detected by a DLTS peak at $E_v + 0.38$ eV,⁴³ local-mode absorption [$C(3)$ center],⁴⁹ and ir electronic absorption or luminescence at 0.79 eV (C line).⁵⁰ In p -type material, an EPR spectrum, Si-G15,⁵¹ has been shown recently to arise from the ionized donor state of the same defect complex as gives rise to the 0.79 -eV C -line luminescence and DLTS peak at $E_v + 0.38$ eV, allowing a microscopic identification of the defect as a simple $C_i O_i$ pair.³⁹

In n -type material, however, the picture of carbon-associated defects has not been clear. There was an early tentative assignment of an $E_c - 0.10$ eV DLTS peak to the acceptor state of the isolated C_i defect^{52,53} and very recent DLTS studies^{17,18} have provided evidence that the bistable $E_c - 0.17$ eV Jellison center may be identified with an acceptor state of the $C_i C_s$ pair. DLTS evidence for the pairing of C_i with substitutional group-V donors has also recently been cited.^{17,18,25,54} Until the present paper and the one immediately preceding it,³⁶ however, no “microscopic” evidence of these assignments has been available. In the preceding paper,³⁶ the identification by EPR of the ionized C_i^- acceptor has supplied the first such direct evidence, confirming the $E_c - 0.10$ eV level assignment.

IV. THE BISTABLE $C_i C_s$ PAIR

The microscopic identification of an acceptor state of the isolated carbon interstitial opens up the possibility of monitoring and identifying other carbon-related defects in n -type silicon. As was previously known in p -type material, a product of C_i^+ (Si-G12) (Ref. 41) anneal is the ($C_i C_s$)⁺ pair (Si-G11) (Ref. 46) in FZ material, and the ($C_i O_i$)⁺ pair (Si-G15) (Ref. 51) in Cz material. Similar reactions are expected in n -type material. If the resulting defect complexes also have acceptor states, they should also be observable in both DLTS and EPR.

A. DLTS studies in n type

In an earlier DLTS study,¹⁸ we established that the bistable Jellison $E_c - 0.17$ eV center is one of two direct products when a precursor $E_c - 0.10$ eV peak anneals at 300 – 350 K. In the preceding paper,³⁶ we have established that the precursor $E_c - 0.10$ eV DLTS peak arises from isolated interstitial carbon in its single-acceptor state (C_i^-). We can conclude, therefore, that the bistable $E_c - 0.17$ eV center is carbon-related. This is consistent with our earlier studies¹⁸ where we demonstrated that the production rate of the bistable defect is proportional to $[C]$ in the sample, but not $[O]$. With correlative EPR studies, we also showed that the well-characterized oxygen-vacancy ($O-V$) pair (A -center) defect is not related to this bistable defect. This served to rule out the pre-

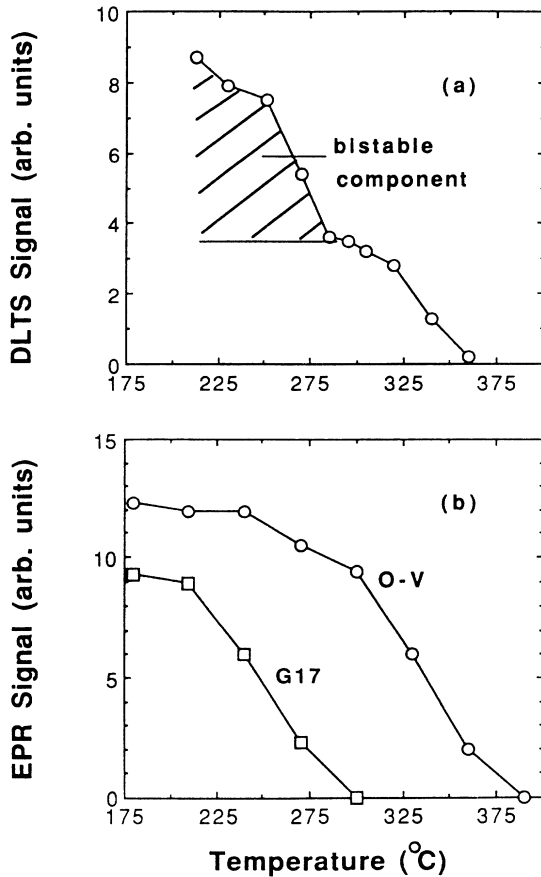


FIG. 2. (a) Isochronal anneal (15 min) of the two components of the $E_c - 0.17$ eV DLTS level (sample No. 2). (b) Isochronal anneal (15 min) of the Si-G17 and the O-V pair EPR spectra for sample No. 2.

vious suggestion that the $E_c - 0.17$ eV bistable defect might be related to oxygen or the O-V pair.^{11,14}

In Fig. 2(a), we show our annealing results for the $E_c - 0.17$ eV level in sample No. 2 that contained both O-V pairs (observed by EPR) and the bistable center. Consistent with the observation of Jellison, the bistable component anneals out first, closely matching that reported for the $(C_i C_3)^+$ pairs in the EPR Si-G11 studies.⁴¹ The O-V pairs provide the stable component which anneals out at higher temperatures.^{33,37} This, plus the dependence upon carbon concentration, led us to our original suggestion that the bistable $E_c - 0.17$ eV defect is a carbon-carbon pair, arising from the single-acceptor level ($-/0$) of the defect.¹⁸ This conclusion was also independently arrived at using similar arguments by Asom *et al.*¹⁷

In our DLTS studies, we find that there are several ways to generate the metastable $E_c - 0.10$ eV level of the Jellison center. In addition to cooling down under reverse bias,^{11,14,18} it can also be generated by minority carrier injection at $T < 50$ K, regardless of cooling conditions. Either forward bias injection or photoexcitation with Nd:YAG (1.16 eV) light is effective. This observa-

tion will have important bearing on the EPR experiments to follow.

B. EPR studies in n type

1. EPR spectra

In the preceding paper,³⁶ an EPR spectrum labeled Si-L6 was identified as arising from the negatively charged state of isolated interstitial carbon (C_i^-). Accompanying its anneal at 300–350 K, another EPR spectrum is observed to emerge with 1:1 correspondence. It is labeled Si-G17, reported previously but not identified.⁵¹ The Si-G17 spectrum was studied at $T \sim 30$ K in dispersion and in the slow passage case⁵⁵ in order to get better resolution, as shown in Fig. 3(a). The appropriate spin Hamiltonian is given by

$$\mathcal{H} = \mu_B \mathbf{B} \cdot \mathbf{g} \cdot \mathbf{S} \quad (3)$$

with $S = \frac{1}{2}$. The angular dependence of the spectrum is shown in Fig. 3(b). The spectrum has C_{1h} symmetry with

$$\begin{aligned} g_1 &= 2.0001 \pm 0.0002, \\ g_2 &= 2.0021 \pm 0.0002, \\ g_3 &= 2.0027 \pm 0.0002, \\ \theta &= 16 \pm 2^\circ. \end{aligned} \quad (4)$$

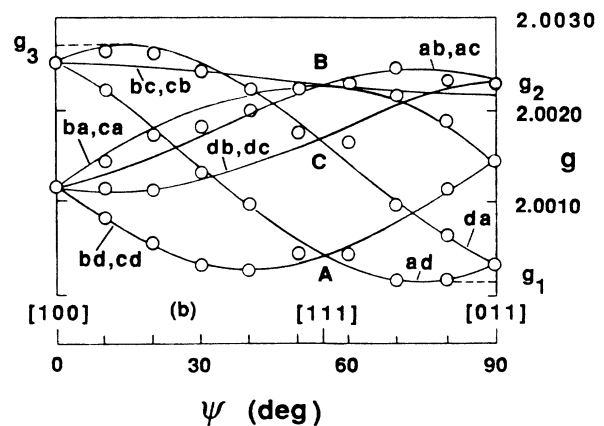
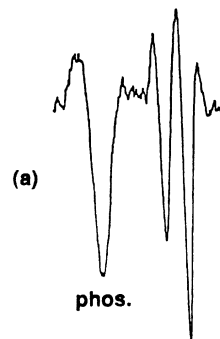


FIG. 3. (a) Si-G17 spectrum at $\nu = 14.182$ GHz, $\mathbf{B} \parallel [100]$, $T \sim 30$ K. The low-field phosphorus donor resonance is also present. (b) Angular dependence of the Si-G17 spectrum g values. The defect axes and resonance line labeling are defined in Fig. 4.

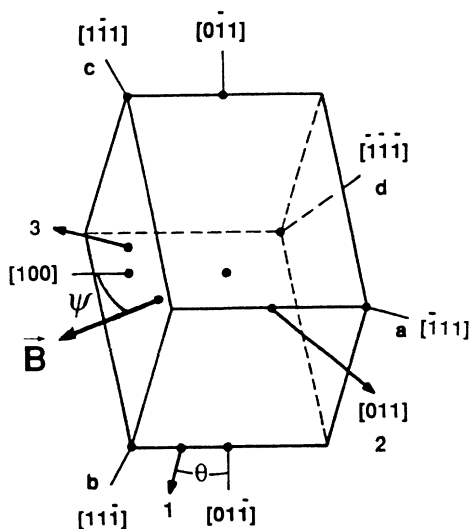


FIG. 4. Principal axes used for the spin-Hamiltonian parameters of the EPR spectra in this study.

The defect axes are given in Fig. 4.

In Fig. 3(b), the differently oriented defects associated with each branch of the spectrum have been denoted in the usual convention⁵⁶ by two letters, each of which refers to one of the four $\langle 111 \rangle$ axes as illustrated in Fig. 4. The first letter specifies the $\langle 111 \rangle$ axis closest to the g_3 axis, and the second letter specifies the $\langle 111 \rangle$ axis closest to the g_1 axis. In Fig. 4, the specific defect axes illustrated correspond to defect *cb*.

There are no resolved ^{29}Si hyperfine satellites associated with a single silicon atom up to ± 0.02 T, which indicates that the defect is not a vacancy-related dangling-bond type center.⁵¹ The energy-level position of the Si-G17 center was estimated to be deeper than the phosphorus donor but shallower than the O-V pair ($E_c - 0.045$ eV $< E_t < E_c - 0.17$ eV), by monitoring the growth and decay of the P, Si-G17, and O-V EPR spectra versus irradiation dose, as was described in more detail in the preceding paper³⁶ for the Si-L6 center. This is in the general region where the $E_c - 0.17$ eV DLTS peak emits. The true energy-level position of this defect will be discussed in Sec. VI C.

In Fig. 2(b) we show annealing results for the Si-G17 and O-V EPR spectra in a sample from the same boule (No. 2) as that used for the DLTS annealing results in Fig. 2(a). The similarity between the two sets of results strongly suggests that the Si-G17 spectrum arises from the same defect that gives rise to the bistable $E_c - 0.17$ eV level in the DLTS studies. The critical test for this identification, however, is whether the bistability is also manifested in the EPR. We find indeed that there is evidence of a second configuration for the Si-G17 center. By injecting with Nd:YAG laser light at $T \leq 50$ K for a few minutes, we find that a new EPR center, labeled Si-L7, emerges with 1:1 correspondence as the Si-G17 disappears. The conversion follows a simple exponential func-

tion of time under a fixed injection laser power density.

The spectrum of Si-L7 is shown in Fig. 5(a) at $T \sim 30$ K. It is observed in the slow passage case⁵⁵ similar to that for Si-G17 indicating that the spin lattice relaxation times for the two centers are comparable. Again, no resolvable hyperfine interaction is observed from a single ^{29}Si atom up to ± 0.02 T. The Si-L7 spectrum has some interesting additional features, however. At $T \geq 15$ K, analysis of the spin Hamiltonian [Eq. (3)] with $S = \frac{1}{2}$ indicates that the spectrum is axially symmetric along a $\langle 111 \rangle$ axis (C_{3v} point-group symmetry corresponding to $\theta = 35.3^\circ$ in Fig. 4). The angular dependence of the spectral lines are shown in Fig. 5(b). The g values are measured to be

$$\begin{aligned} g_{\parallel} &= 2.0008 \pm 0.0002, \\ g_{\perp} &= 1.9994 \pm 0.0002. \end{aligned} \quad (5)$$

The lines plotted in Fig. 5(b) represent the positions of the spectral lines as calculated using these g values. (For a C_{3v} -symmetry center, only the first letter of our labeling convention is required.) The spectrum also shows an unusual satellite structure, as seen in the figure, which matches well that predicted for equal ^{29}Si hyperfine coupling ($I = \frac{1}{2}$, 4.7% abundance) with ~ 24 silicon neighbors.

When $T < 15$ K, the lines of the spectrum broaden and

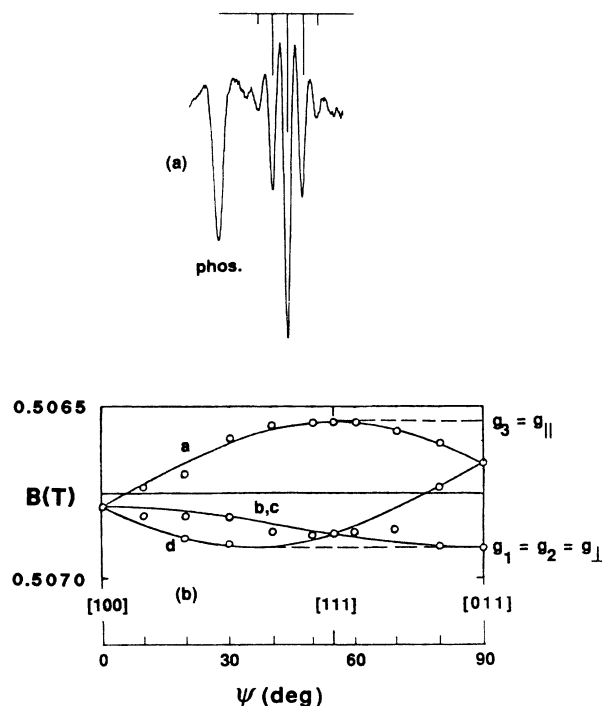


FIG. 5. (a) Si-L7 spectrum at $\nu = 14.182$ GHz, $\mathbf{B} \parallel [100]$, and $T \sim 30$ K, also showing the satellite structure expected for ^{29}Si hyperfine interaction with ~ 24 equivalent sites. (b) Angular dependence of the Si-L7 spectrum measured at $T \geq 15$ K. The defect axes are defined in Fig. 4.

the satellite structure disappears, indicating that the symmetry of the center is lowered. This suggests that the center at $T \geq 15$ K is in a motionally averaged state. No static lower symmetry spectrum could be frozen out even at $T \sim 2$ K, however. Applying uniaxial stress (41 MPa) at these low temperatures was unsuccessful in an attempt to sharpen the lines.

Actually, all three of the carbon-related spectra (Si-L6, Si-G17, Si-L7) behave in an unusual fashion at low temperature. At $T \sim 35$ K for Si-L6 and $T \sim 20$ K for Si-G17 and Si-L7, the maximum signal is seen 90° out of phase with the modulation, which is the characteristic of a rapid passage case with $\omega_m T_1 \sim 1$.⁵⁵ As the temperature is lowered, the intensities of the 90° out-of-phase spectra decrease as expected, but the 0° in-phase mode never gets strong as expected for $\omega_m T_1 \gg 1$. The reason for this is not understood. It may indicate that the spin-spin relaxation time T_2 (which determines the spin packet width) remains short, perhaps resulting from some residual motion for each of the centers, preventing proper adiabatic rapid passage conditions.

The Si-L7 spectrum is only stable thermally at low temperature. Upon heating the sample in the dark to ~ 50 K, the Si-L7 spectrum disappears and the Si-G17 spectrum returns. The recovery follows a simple exponential form and the time constant measured versus temperature is given by

$$\tau = 6.4 \times 10^{-13} \exp[(0.15 \text{ eV})/kT]. \quad (6)$$

2. Bistability between Si-G17 and Si-L7

For the samples we have discussed so far, the electron irradiation dose was such that the Fermi level remained above the Si-G17 acceptor level (still locked on the phosphorus donors). This means that all the defects had a trapped electron when the sample was cooled down in the dark, and therefore the Si-G17 spectrum arises from the stable configuration when charged. The stable configuration (Si-G17) converts to a metastable configuration (Si-L7) under photoinjection, as sketched in Fig. 6(a). The charge state cannot have changed in the process because both centers have $S = \frac{1}{2}$. The reverse process (Si-L7 \rightarrow Si-G17) was achieved thermally by heating the sample in the dark. This conversion process [Eq. (6)] is plotted as an extension of the data of Jellison for the $E_c - 0.11$ eV to $E_c - 0.17$ eV conversion under zero bias,¹³ as shown in Fig. 7, with excellent agreement. One can cycle back and forth repetitively between the two EPR centers in exact correlation with the corresponding electrical or optical injection and thermal recovery experiments in the DLTS studies. This demonstrates, therefore, that the two EPR centers we have observed, Si-G17 and Si-L7, are associated with the two configurations of the Jellison DLTS center at $E_c - 0.17$ eV (A^-) and $E_c - 0.11$ eV (B^-), respectively, when charged.

At this point we have not yet established the actual net electrical charge on the defects when they have trapped an electron. For convenience in the presentation that follows, however, we will label the defects as negatively charged in this case, as originally proposed by Chantre

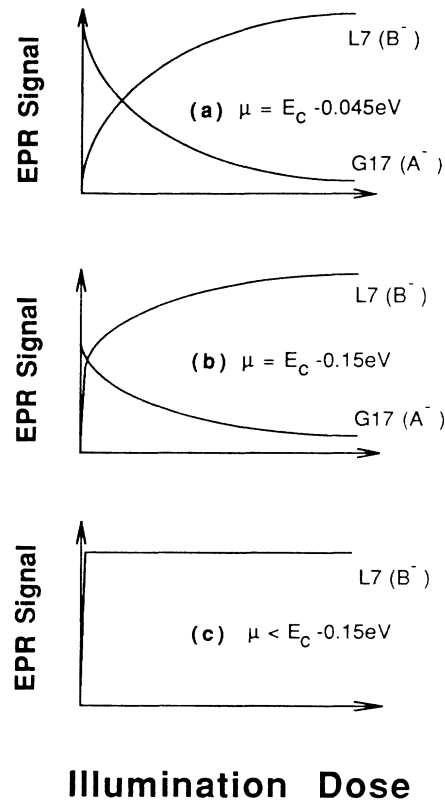
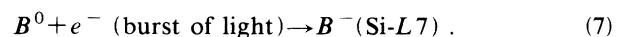


FIG. 6. Schematic drawing of the effect of photoinjection at $T \leq 50$ K on the intensities of the Si-G17 and Si-L7 EPR spectra as a function of the Fermi energy μ .

*et al.*¹¹ and described by the configurational coordinate diagram in Fig. 1. (At the end of this section when all of the experimental results have been presented we will be able to demonstrate that this assignment is correct.) Following this scheme, Si-G17 arises from configuration A^- and Si-L7 from B^- , the corresponding single acceptor ($-/0$) levels being located at $E_c - 0.17$ eV and $E_c - 0.11$ eV, respectively.

Now if we irradiate the sample further so that the Fermi level is locked on the Si-G17 acceptor level (at the conclusion of this paper, Sec. VI C, we will have established that the true acceptor-level position is at $E_c - 0.15$ eV), then under thermodynamic equilibrium, part of the defects are charged (A^-) and part are neutral (stable in B^0). EPR only shows the charged defects (Si-G17), since the neutral ones are nonparamagnetic. Now if we shine a burst of light (Nd:YAG laser) at $T < 40$ K, the photogenerated electrons can be trapped by the B^0 defects to produce B^- which are paramagnetic (Si-L7). Subsequent prolonged injection should convert the initial A^- (Si-G17) to B^- (Si-L7) but at a much slower rate. This is indeed observed, as illustrated schematically in Fig. 6(b), where the initial increase of the Si-L7 signal serves as a measure of the equilibrium concentration of B^0 , i.e.,



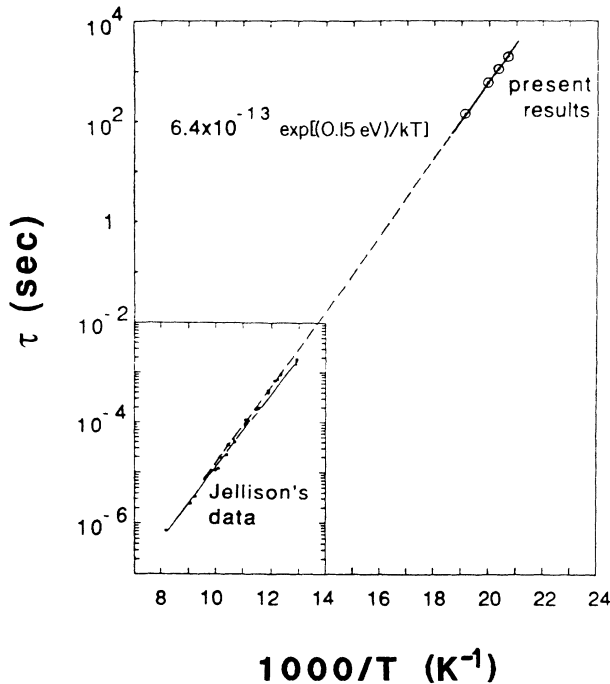


FIG. 7. Temperature dependence of the Si-L7→Si-G17 conversion time constant plotted as an extension of the data of Jellison (Ref. 13), indicating that the same process is being monitored.

After further electron irradiation, when the Fermi level is below $E_c - 0.15$ eV, all the defects are stable in the B^0 configuration under thermodynamic equilibrium conditions. In such a sample, we detect no Si-G17 (A^-) signal when the sample is cooled down in the dark. However, a burst of light (Nd:YAG) converts the B^0 to B^- (Si-L7), which is detected in the EPR as shown in Fig. 6(c). Subsequent injection does not increase the Si-L7 signal since there were no defects in the A configuration to start with.

In such a sample, the electron trapped on the Si-L7 (B^-) center is not stable since the Fermi level is below the defect level. As the temperature is raised, the electron will therefore be emitted to the conduction band, $B^- \rightarrow B^0 + e^-$ (to be trapped at deeper levels), and the Si-L7 spectrum will disappear. The kinetics of this process have been studied and the results are plotted in Fig. 8, along with the data of Jellison for the $E_c - 0.11$ eV emission.¹³ The two emission processes agree very well. These results demonstrate that the same process is being monitored in both the EPR and DLTS studies.

Therefore, the conclusion is unambiguous that the Si-G17 and Si-L7 EPR spectra arise from the two bistable components of the same defect previously reported in the DLTS studies. All the bistable features fit nicely and accurately to the earlier results.

3. Spectroscopic information from Si-G17

A direct identification of the chemical species involved in a defect center can be established by the presence of

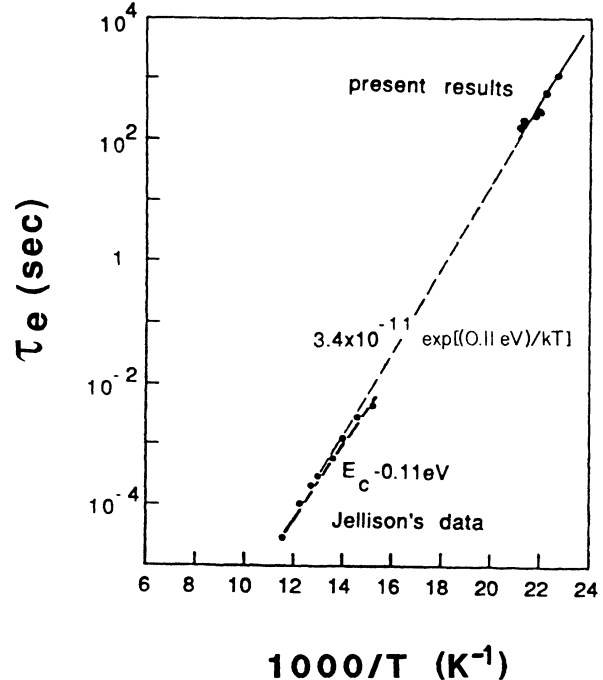


FIG. 8. Electron emission time constant τ_e vs temperature for the Si-L7 center. The results are plotted as an extension of the data of Jellison (Ref. 13), confirming that the same emission process is being measured.

hyperfine interactions in its EPR spectrum. Unfortunately, the natural abundance of ^{13}C is only 1.1% and such structure would be almost impossible to see. In a specially ^{13}C -enriched p -type sample No. 6, however, the ^{13}C isotope had been enriched to $\sim 60\%$. It was converted to n -type material (sample No. 4) using the neutron-transmutation technique.

Irradiating this sample with the proper dose so that the Si-G17 spectrum was at its maximum under thermodynamic equilibrium, we observed additional structure from the spectrum as shown in Fig. 9(b). Compared with a sample with natural abundance carbon and under the same detection conditions, Fig. 9(a), we clearly have more structure from the ^{13}C -enriched sample. Unfortunately, the structure is too poorly resolved to analyze the hyperfine terms in detail. However, computer simulation, with two inequivalent carbon atoms interacting in the center, matches the spectrum very well, as shown in Fig. 9(c).

The simulation was made as follows. It is reasonable to assume that the relative hyperfine line intensities are known since the isotope dopants are 60% ^{13}C and 40% ^{12}C . A Gaussian line shape was generated by computer for each hyperfine line with the linewidth determined from the resolved (normal ^{12}C sample) spectrum. Each hyperfine interaction was then varied so that the corresponding line positions moved as a pair with respect to the central ^{12}C lines. The hyperfine interactions were adjusted until the superimposed spectrum matched the ex-

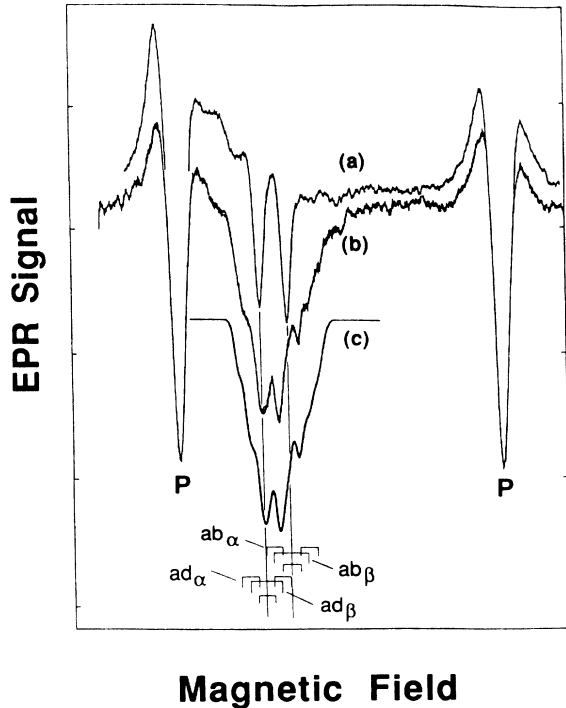


FIG. 9. (a) Si-G17 spectrum in a natural ^{13}C abundance (1.1%) sample (No. 5). (b) Si-G17 spectrum in a ^{13}C (60%)– ^{12}C (40%)–enriched sample No. 4. (c) Computer simulation of the ^{13}C -enriched Si-G17 spectrum for two inequivalent C atoms. The spectra were taken at $T \sim 20$ K with an intermediate phase on the lock-in detector and $\mathbf{B} \parallel [100]$.

perimental one. The simulation was made only with the magnetic field along the $\langle 100 \rangle$ direction of the sample. Two sets of hyperfine interactions α, β (following Brower's notation) (Ref. 46) from two inequivalent carbon atoms split the two central ^{12}C lines [ab and ad , using the labeling scheme in Fig. 3(b)]. Denoting by ab_α the hyperfine splitting on the ab oriented defect arising from atom α , etc., the deduced splittings are shown in Fig. 9(c). They are also given in Table II, together with those measured by Brower for Si-G11 (C_iC_s) $^+$ for comparison. The magnitudes are an order of magnitude weaker but the overall features are very similar. This indicates, as for isolated C_i^- , 36 that the spin wave function is not primarily localized on either of the carbon atoms. This analysis is, of course, only approximate. However, we were not able to simulate the spectrum by a single carbon atom interaction, or by assuming two equivalent carbon atoms.

This provides the first spectroscopic confirmation that the defect giving rise to Si-G17 consists of two inequivalent carbon atoms. The center is therefore in an odd charge state in order to be paramagnetic. It must be associated with a second level of the C_iC_s pair, i.e., the acceptor state ($-/0$) of the C_iC_s pair. Apparently, the distribution of the spin wave function is quite different when the defect is in its acceptor state. It is much less localized on the carbon atoms than that in the donor state.

TABLE II. ^{13}C hyperfine splittings (units in 10^{-4} T) for the two inequivalent carbon atoms with $\mathbf{B} \parallel [100]$ for the Si-G17 and Si-G11 (C_iC_s) $^+$ spectra.

	Si-G17	Si-G11 ^a
$(ab)_\beta / (ad)_\beta$	4.20/3.75	33.6/16.5
$(ab)_\alpha / (ad)_\alpha$	2.20/2.15	12.1/12.6

^a Reference 46.

The bistable partner Si-L7, on the other hand, shows no resolvable ^{13}C hyperfine interaction in this ^{13}C -enriched sample. This indicates that the spin wave function is even less localized on the carbon atoms when the defect is in the B configuration.

There are two types of alignment effects that can be observed in an EPR spectrum due to applied stress. 32 First, the energy of the electron trapped at the defect center is raised or lowered depending upon the orientation of the defect with respect to the stress. The EPR line intensities associated with the differently oriented defects can change therefore as a result of electronic redistribution between the defects if the defects are only partially occupied. Second, the defects may reorient thermally and accumulate in a preferential orientation with respect to the applied stress.

Figure 10 shows the change in the Si-G17 spectrum

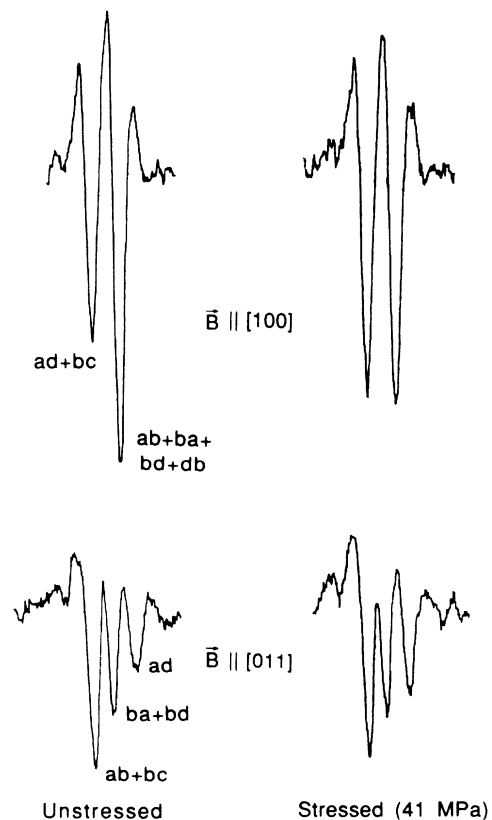


FIG. 10. Effect on the Si-G17 spectrum of cooling from $T \sim 77$ K under $[0\bar{1}1]$ compressional stress.

with $\mathbf{B} \parallel [100]$ and $[011]$ resulting from an applied $[0\bar{1}1]$ compressional stress (~ 41 MPa) at ~ 77 K. In this experiment, the sample was cooled with stress on to the EPR measurement temperature before removing the stress. A very similar quenched-in alignment was reported for the Si-G11 center.⁴⁶ Just as for the Si-G11 center, this alignment can be achieved in the presence of many more electrons than Si-G17 defects (i.e., the Fermi level is still locked on the phosphorus donors). This establishes that the process is not the electronic redistribution between differently oriented defects. The process therefore must be one in which the individual defects reorient.

The actual alignment is only a limited one. We notice that there is not a complete alignment from the fact that the sum of intensities for EPR lines with the same first letter [see angular dependence in Fig. 3(b)] does not change. This indicates that the defect reorientation is limited to the three equivalent distortions around a fixed $\langle 111 \rangle$ axis for the defect. In this case, it is not possible to extract the components of the tensor \underline{B} , conventionally used to describe the coupling of a defect to applied strain.³⁶ Identical behavior was observed for the Si-G11 spectrum.⁴⁶

Isothermal recovery from this alignment was measured as a function of temperature. The result is plotted in Fig. 11, together with the corresponding results for the Si-G11 (C_iC_s)⁺ center.⁴⁶ Although the rates are not identical, they are very close, displaying almost the same activation energy. This, plus the very similar character and degree of alignment, suggests that the core structure of the two centers is essentially the same. In other words, this supplies further confirmation that these spectra arise from different charge states of the same defect [$(C_iC_s)^-$ and $(C_iC_s)^+$] and suggests in addition that they are both

in the same configuration (A).

No alignment was observed for the defect in the B^- (Si-L7) configuration either after applying stress at the measuring temperature (~ 30 K) or by first applying stress at ~ 77 K and then converting by photoinjection to the B configuration at low temperature. (We will see that this makes sense in terms of the final models to be presented in Sec. VI that the B configuration is a saddle point for reorientation among the three equivalent A configurations.)

An attempt to detect the first letter $\langle 111 \rangle$ axis alignment after higher temperature ($\sim 170^\circ\text{C}$) stress and quench to the measuring temperature, as had been observed for the Si-G11 (C_iC_s)⁺ center,⁴⁶ was not successful for either the Si-G17 or Si-L7 centers. This failure may have been due to the anneal of the P-V pair at this stress temperature,⁵⁶ which greatly increased the nearby phosphorus donor resonance (Figs. 3 and 5) making it difficult to detect small changes in the Si-G17 and Si-L7 spectra.

C. EPR studies in p type

The conclusion in the last section that both $(C_iC_s)^-$ and $(C_iC_s)^+$ have A as their stable configuration indicates that the bistability observed for $(C_iC_s)^-$ should also apply to $(C_iC_s)^+$, since the stable B configuration for $(C_iC_s)^0$ is adjacent to both. In EPR studies, the most effective way to explore this, as has been shown in the n -type sample, is again to use the Nd:YAG laser as a photoinjection source. By monitoring the Si-G11 spectrum in a p -type sample, we do indeed observe a simple exponential decay of the spectrum with increasing injection time at the EPR measurement temperature (~ 15 K). This is consistent with a configurational change. No new EPR center was detected, however, when the Si-G11 center disappeared. (In the search, we have covered the temperature range 2–50 K.)

To measure the recovery of Si-G11 (A^+), a series of isothermal annealings were performed in the temperature range 60–65 K. The recovery time was measured to be

$$\tau = 2 \times 10^{-14} \exp[(0.21 \text{ eV})/kT]. \quad (8)$$

Again, this is the characteristic behavior of a bistable defect for which a thermal barrier exists between the two configurations.

From experiments monitoring the EPR intensities versus irradiation dose in the p -type material, we are led to conclude that the energy-level position of $(C_iC_s)^+$ is shallower than that for the divacancy $(V-V)^+$ (Si-G6 EPR center).⁵⁷ This is shown in Fig. 12 where the Si-G11 center is decreasing while the Si-G6 center still increases. This means that under thermodynamic equilibrium the holes are more loosely bound to the Si-G11 center than on the Si-G6 center. Energetically, therefore, the Si-G11 center is shallower than Si-G6. This is inconsistent with the previous DLTS assignments⁴² of $E_v + 0.33$ eV for the C_iC_s donor level and $E_v + 0.21$ eV for the divacancy level. Actually, the assignment of a level at $\sim E_v + 0.2$ eV to the $(V-V)^+$ defect⁴² is more reliable since various in-

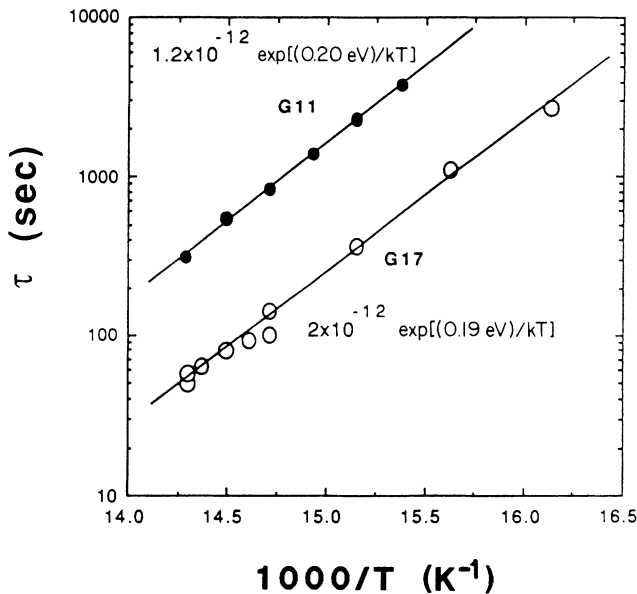


FIG. 11. Time constant vs temperature for the recovery from 77 K stress alignment for the Si-G17 spectrum, together with that from a similar study for the Si-G11 center (Ref. 46).

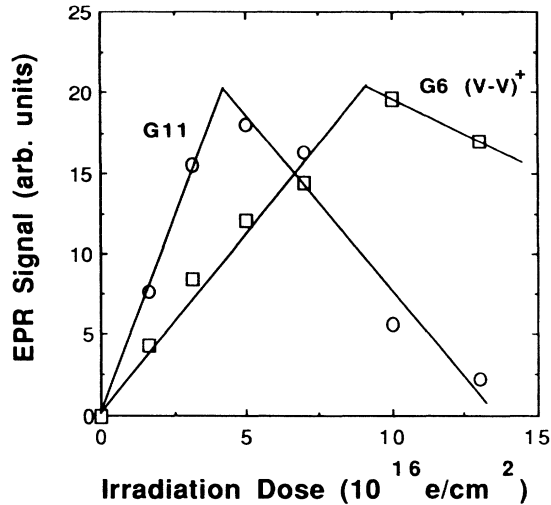


FIG. 12. EPR signal intensities as a function of 2.5 MeV electron irradiation dose in a p -type sample (No. 5), showing that the energy-level position of the Si-G11 center is shallower than the Si-G6 center.

dependent techniques have been employed to estimate the level position^{57,58} including Hall measurements.⁵⁹ Hall measurements monitor the carrier concentration under thermodynamic equilibrium when the Fermi level is locked to the defect and therefore, properly interpreted, measure the true electrical level position. As will be discussed in the next section we will find that the $E_v + 0.33$ eV assignment was incorrect.

So far, we have provided strong evidence that the metastable B configuration can also be produced in p -type samples. There is no direct observation, however, from EPR experiments of this configuration in the p -type material. One possibility is that the donor level for the B configuration is below the valence-band edge so that B^+ is not stable. Another explanation is that B^+ does exist in the band gap, but its donor level either has an extremely small hole capture cross section or is too shallow for B^+ to be detected by EPR.^{60,61} To differentiate between these possibilities, we must better understand the electrical properties of the $(C_iC_s)^+$ center. That requires other techniques such as DLTS.

D. DLTS studies in p type

The earlier assignment of a DLTS peak at $E_v + 0.33$ eV to hole emission from $(C_iC_s)^+$ was made based on the observation that this peak grew in with 1:1 correspondence when C_i^+ ($E_v + 0.28$ eV) annealed around 300–350 K.⁴² The sample used in that DLTS study was made by a diffusion process, however, which in general introduces oxygen into the junction. It was noted in a subsequent study⁴³ that the $E_v + 0.33$ eV peak annealed around 400°C, much higher than $(C_iC_s)^+$ ($\sim 300^\circ\text{C}$).

The DLTS samples used in this study (Table I) were low-oxygen materials. Either ion-implantation or Schottky-barrier processing was employed to make sure

no additional oxygen was incorporated into the junction. In these samples, we detected no peak at $E_v + 0.33$ eV after C_i^+ ($E_v + 0.28$ eV) annealed at 300–350 K. Instead, a new emission at $E_v + 0.09$ eV was detected with emission time constant

$$\tau = 1.6 \times 10^{-13} \exp[(0.086 \text{ eV})/kT]. \quad (9)$$

As plotted in Fig. 13, $\sim 70\%$ of the $E_v + 0.28$ eV level intensity was converted to the $E_v + 0.09$ eV level in this sample. Most of the remainder can be accounted for by the decrease of the divacancy signal, which may result from the trapping of the C_i to annihilate the divacancy defects. The hole capture cross section of the $E_v + 0.09$ eV peak was measured to be $\sigma_p \geq 10^{-16} \text{ cm}^2$.

This DLTS peak shows bistability, as shown in Fig. 14. Cooling down under zero bias, the $E_v + 0.09$ eV level is stable. Cooling down under reverse bias, or with minority carrier injection at $T \leq 50$ K, independent of cooling bias condition, the $E_v + 0.09$ eV level almost disappears. This is a very similar situation as that for the EPR Si-G11 spectrum under photoinjection. No new DLTS peak was detected when the $E_v + 0.09$ eV level disappeared.

The annealing of the $E_v + 0.09$ eV peak ($\sim 300^\circ\text{C}$, 15 min) is very similar to the Si-G11 center. We can conclude therefore that the $E_v + 0.09$ eV level is directly associated with the Si-G11 center. In other words, the donor state of the C_iC_s pair has an energy level at $E_v + 0.09$ eV, not $E_v + 0.33$ eV as suggested before.⁴² The misidentification, we believe, was due to oxygen incorporated into the junction during the diffusion junction process. The peak at $E_v + 0.33$ eV must result from the C_iO_i defect which has been reported to introduce an energy level in this region.⁴³

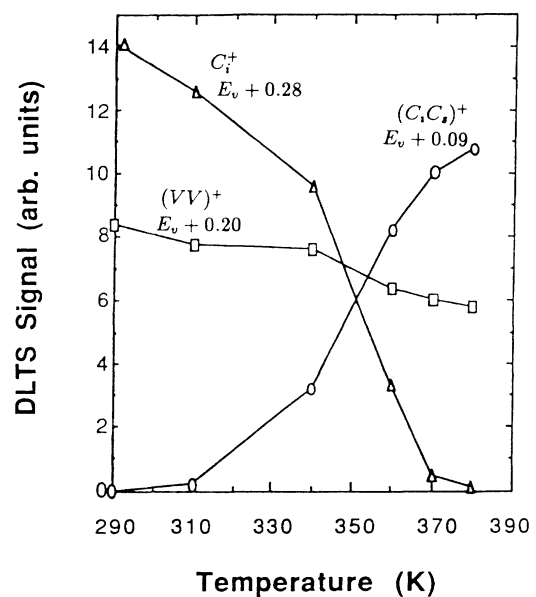


FIG. 13. Defect concentrations measured by DLTS during isochronal annealing (15 min) in a p -type sample (No. 5).

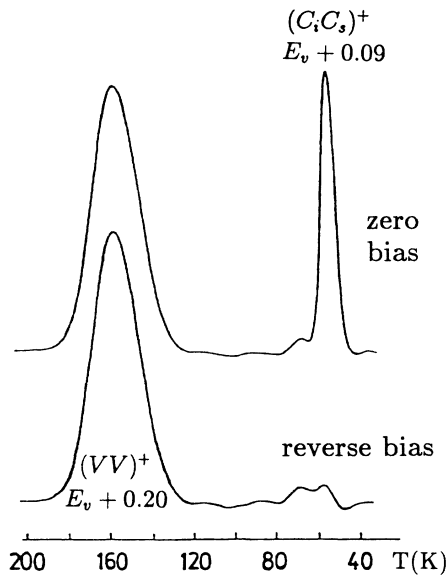


FIG. 14. Bistability of the $E_v + 0.09$ eV level. It is only stable under zero-bias cooling.

With the $E_v + 0.09$ eV peak, we can measure the interconversion between the two configurations of the $(C_i C_s)^+$ defect. As plotted in Fig. 15(a), the $B^+ \rightarrow A^+$ conversion was measured by cooling the sample under reverse bias and then isothermal annealing at 60–70 K under zero bias. This result agrees satisfactorily with the Si-G11 EPR signal recovery, Eq. (8). This confirms that the same process is being measured by both EPR and DLTS, and that the $E_v + 0.09$ eV peak results from hole emission

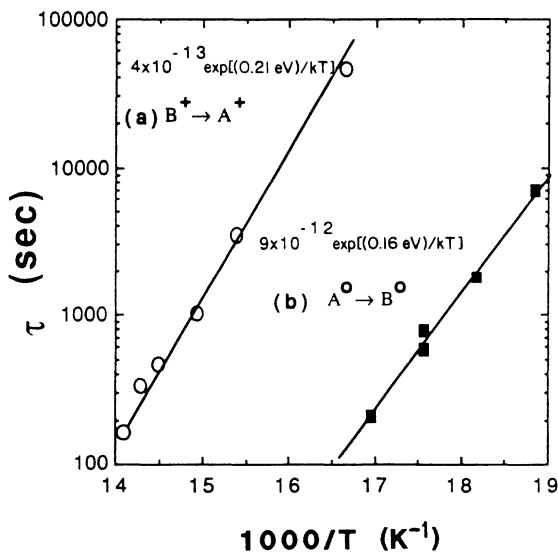


FIG. 15. Time constant vs temperature for the conversion between the A and B configurations by monitoring the $E_v + 0.09$ eV peak. (a) $B^+ \rightarrow A^+$ conversion, under zero bias. (b) $A^0 \rightarrow B^0$ conversion, under reverse bias.

from $(C_i C_s)^+$. The reverse bias conversion $A^0 \rightarrow B^0$ was also measured, as given in Fig. 15(b), which indicates that the thermal barrier in the neutral charge state is ~ 0.16 eV.

From Fig. 14 we also note that reverse bias cooling does not convert all of the defects to the B configuration, a small contribution of A remains. The amplitude of the $E_v + 0.09$ eV peak under reverse bias was found to be a function of the temperature at which equilibrium between A^0 and B^0 was quenched in. Figure 16 shows the equilibrium ratio

$$\frac{[B^0]}{[A^0]} = \frac{(N_B)_{RB}}{(N_A)_{RB}} = \frac{(N_A)_{ZB} - (N_A)_{RB}}{(N_A)_{RB}} \quad (10)$$

estimated for three different quenching temperatures. The temperature dependence of this ratio confirms our interpretation that the weak residual peak at $E_v + 0.09$ eV under reverse bias cool down does indeed arise from $C_i C_s$ in the A configuration. The slope gives the energy difference between the A^0 and B^0 minima to be ~ 0.017 eV.

E. PL studies in n and p type

With the combination of DLTS and EPR techniques, we have obtained almost all of the relevant energy values for the three energy surfaces of the $C_i C_s$ pairs. In the A configuration, the EPR active centers in both $(C_i C_s)^-$ and $(C_i C_s)^+$ charge states reveal detailed microscopic structural information about the core of the defect. However, the B configuration is stable in the neutral charge state and therefore is nonparamagnetic. We therefore have no direct spectroscopic information from EPR associated with the B configuration except the metastable state B^- (Si-L7 center).

As mentioned in Sec. III, an optical transition has been observed in both absorption and emission with zero-phonon line at 0.97 eV (Refs. 26–28) which arises from a

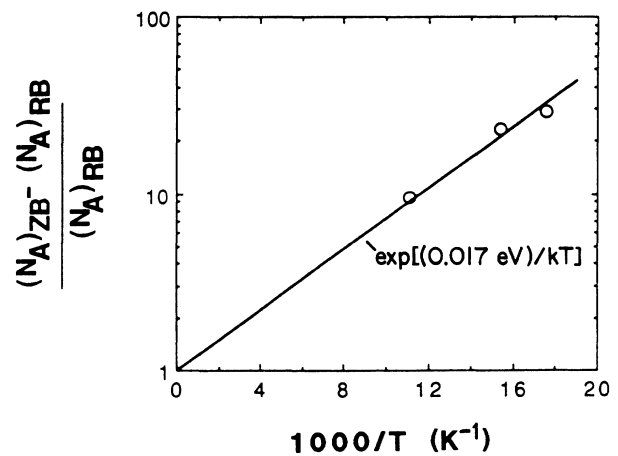


FIG. 16. The equilibrium ratio $[B^0]/[A^0]$, estimated from the height of the $E_v + 0.09$ eV DLTS peak under zero and reverse bias, Eq. (10), as a function of quenching temperature.

C-C complex as confirmed by ODMR studies.^{47,48} Zeeman studies show that its ground state has $S=0$ consistent with a neutral charge state, as is usually the case at low temperature under photoillumination.⁶² Therefore if a connection can be established between this C-C optical center and the bistable C_iC_s pair, we will now have a spectroscopic means of monitoring all three charge states. In order to make this connection, bistability is again the obvious key. The 0.97-eV luminescence has been studied by many workers. If it has bistable properties, it has been overlooked in all of these previous studies.

1. *n* type

The Nd:YAG laser was used as the excitation source to excite the bulk luminescence and allowed us to make a direct quantitative correlation with the EPR experiments. With a low resistivity sample, i.e., the sample was irradiated in such a way that the Fermi level was above the C_iC_s acceptor level (locked to the phosphorus donor at $E_c - 0.045$ eV), we first cooled the sample down in the dark, so that all the $(C_iC_s)^-$ defects were in the A configuration. We then turned on the excitation light with the monochromator preset at the wavelength of the 0.97 eV luminescence. No luminescence was present initially. Instead, the luminescence intensity grew with illumination time, as shown in Fig. 17(a). The growth rate agrees with the simple exponential function $(1 - e^{-t/\tau})$.

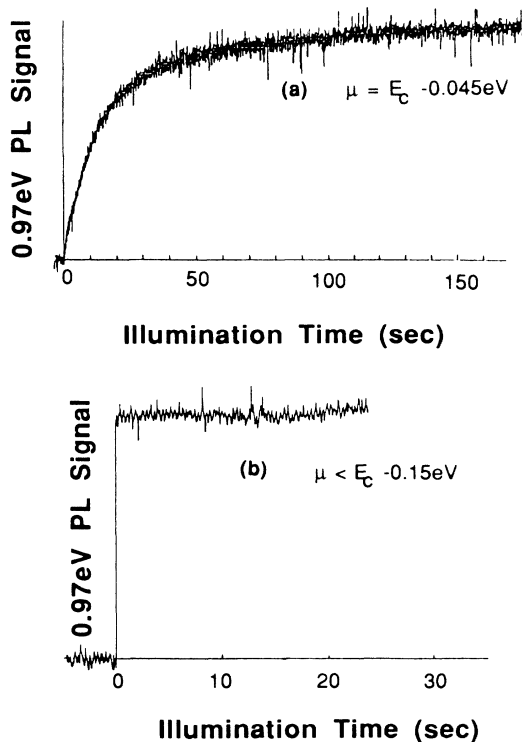


FIG. 17. The intensity of the 0.97-eV luminescence as a function of Nd:YAG laser illumination time in *n*-type samples. (a) The Fermi energy is at the $E_c - 0.045$ eV (phosphorus donor) level. (b) The Fermi energy is below the $E_c - 0.15$ eV level.

These results strongly suggest that the A configuration does not luminesce, and a change to the B configuration is necessary for the 0.97-eV luminescence.

In order to make a direct quantitative correlation between the PL experiment and the EPR work, we measured the growth rate τ^{-1} in the PL versus excitation light intensity, as plotted in Fig. 18(a). One point from the EPR experiment for the $A \rightarrow B$ conversion in the same sample is also shown in the figure. The results agree well within the accuracy of the illumination intensity determination in the two different experimental geometries. The thermal recovery rate for $B^- \rightarrow A^-$ as monitored by PL was also measured and is plotted in Fig. 18(b) together with the $B^- \rightarrow A^-$ rate determined from the EPR studies, Eq. (6). The experiments were performed as follows: After generation of the B configuration by laser excitation, the defects remain in the B configuration even after the excitation is turned off, so long as the sample temperature does not exceed ~ 50 K where the thermally activated $B^- \rightarrow A^-$ recovery process occurs. Subsequent isothermal anneal in the dark in this temperature region converts the defect back to the A configuration. This conversion was monitored by measuring the initial luminescence intensity (B configuration) after each anneal. The similar rates and activation barriers, as shown in Fig. 18(b), indicate that the identical process was monitored by the two different experimental techniques.

To further confirm that the 0.97-eV luminescence is from the B configuration only, we took a sample which was heavily irradiated so that the Fermi level is below the $E_c - 0.15$ eV level. All the defects in this sample were therefore stable in the B^0 configuration when cooled down in the dark. We found indeed that there is no delay in observing the luminescence after turning on the excitation, as shown in Fig. 17(b). This confirms directly that the B configuration is responsible for the 0.97-eV luminescence.

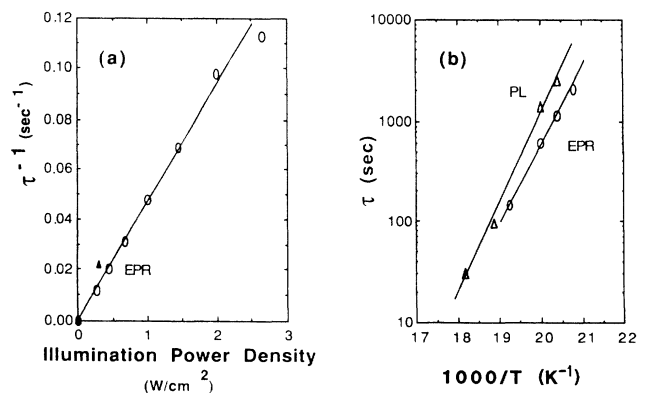


FIG. 18. (a) The growth rate of the 0.97-eV luminescence (\circ) vs Nd:YAG laser power density compared to the $A^- \rightarrow B^-$ conversion rate determined from EPR studies (\blacktriangle) in an *n*-type sample. (b) Time constant for the $B^- \rightarrow A^-$ recovery monitored by PL (\triangle) and EPR (\circ).

2. *p* type

A very similar bistability was observed in *p*-type samples as well, when the C_iC_s defects were initially in the stable *A* configuration. In a lightly irradiated sample (boron doped), the same growth of the 0.97-eV luminescence was detected associated with the configuration change from *A* to *B*, as shown in Fig. 19(a). These experiments were somewhat more difficult because of a strong broad luminescence band which was superimposed on the 0.97-eV luminescence in the *p*-type material. The origin of this broad band, which decreases as the sample temperature increases and disappears at $T \sim 30$ K, is not known. We found, however, that this broad luminescence band was constant versus time, and we could therefore simply subtract its intensity from the total luminescence intensity at 0.97 eV. The resulting transition, as shown in Fig. 19(a), reflects the bistable conversion $A \rightarrow B$, from which the 0.97 eV luminescence originates.

Just as in the *n*-type sample, we measured the $A \rightarrow B$ transition rate as a function of excitation intensity, and also the thermal recovery from $B \rightarrow A$. The results are plotted in Figs. 20(a) and 20(b), together with the corresponding excitation and recovery data, Eq. (8), from EPR. The agreement again is very good.

We have therefore confirmed directly and unambigu-

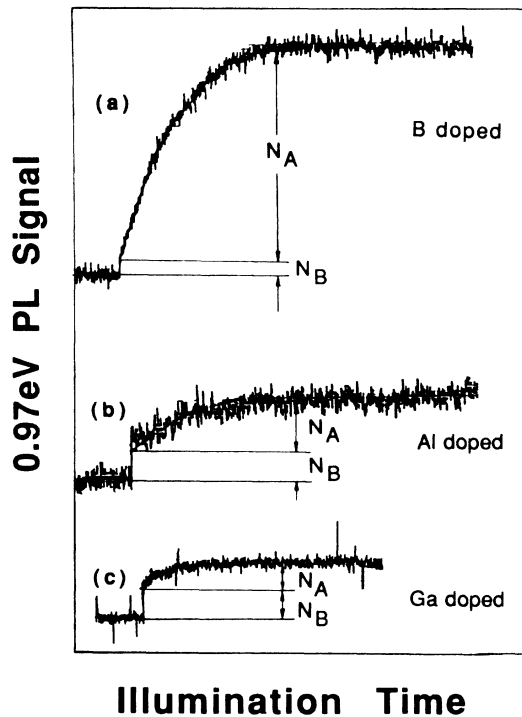


FIG. 19. The growth of the 0.97-eV luminescence intensity vs Nd:YAG laser illumination time: (a) in a B-doped sample ($\mu \sim E_V + 0.0476$ eV at $T = 70$ K), (b) in an Al-doped sample ($\mu \sim E_V + 0.0654$ eV at $T = 70$ K), and (c) in a Ga-doped sample ($\mu \sim E_V + 0.0692$ eV at $T = 70$ K). The initial concentration ratios N_A/N_B were estimated: ~ 14 (B); ~ 2.3 (Al); ~ 1.2 (Ga).

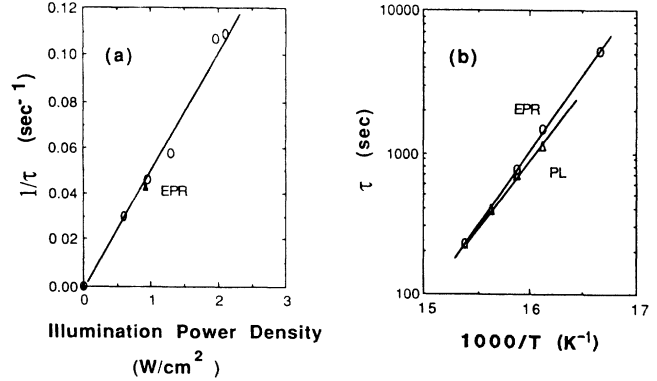


FIG. 20. (a) The $A \rightarrow B$ conversion rate vs Nd:YAG laser power density in a *p*-type (B-doped) sample (\circ , PL; \blacktriangle , EPR). (b) The $B \rightarrow A$ thermal recovery time constant vs temperature (\triangle , PL; \circ , EPR).

ously that the 0.97-eV luminescence arises from the same C_iC_s bistable center seen by EPR and DLTS, and we have obtained important new information that it arises from the *B* configuration only.

From Fig. 19(a) we notice that in this boron-doped low resistivity *p*-type sample there is a weak initial 0.97-eV luminescence which reveals therefore the presence of a certain number of defects initially in the *B* configuration. The additional luminescence that grows in is a measure of the defects initially in the *A* configuration. This initial ratio of $[A]/[B]$, resulting from thermodynamic equilibrium in the dark with the Fermi level close to the boron acceptor level, contains information therefore about the relative energies of the A^+ and B^+ minima. In this lightly irradiated sample, the Fermi level was locked close to the shallow acceptor level at 0.0456 eV above the valence band.⁶³ To investigate the effect of the Fermi level, we studied Al- (and Ga-) doped samples which provide deeper shallow acceptor levels at ~ 0.070 eV (and at ~ 0.074 eV).⁶³ We found indeed that the $[A]/[B]$ ratio decreases as the Fermi-level position moves up, as shown in Figs. 19(b) and 19(c). The ratio of the number of the defects in *A* (N_A) and *B* (N_B) under thermal equilibrium with the Fermi level μ can be derived to be⁶⁴

$$\frac{N_A}{N_B} = \exp(-\Delta E_{AB}^0/kT) \left[\frac{1 + \exp(\Delta E_A - \mu)/kT}{1 + \exp(\Delta E_B - \mu)/kT} \right], \quad (11)$$

where ΔE_{AB}^0 is the energy difference between the A^0 and B^0 minima, and ΔE_A and ΔE_B are the hole ionization activation energies from A^+ and B^+ , respectively. The Fermi energy μ can be determined from the shallow-acceptor energy-level position, its concentration, the deep-donor partial compensation, and the temperature.⁶⁴ Experimentally, we estimated the deep-donor partial compensation by monitoring the carrier removal and deep-level concentration as a function of irradiation dose by DLTS and EPR experiments. In these particular samples, the partial compensation was estimated in this

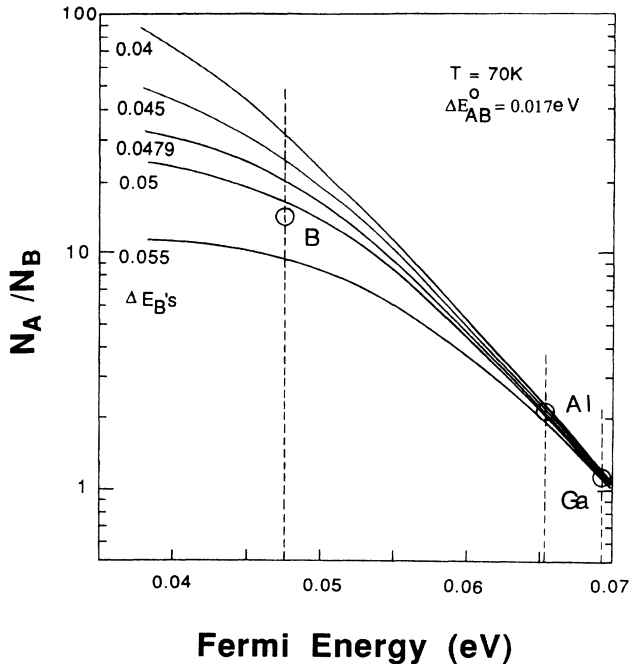


FIG. 21. A plot of Eq. (11), (N_A/N_B) vs the Fermi energy μ for different values of ΔE_B , the hole ionization energy from B^+ . The circled points, determined from Fig. 19, give $\Delta E_B = 0.050 \pm 0.005$ eV.

manner to be $\sim 7\%$ for the B-doped sample and $\sim 10\%$ for the Al- and Ga-doped samples. The Fermi energy μ was determined at $T = 70$ K which is the temperature at which we estimate that the N_A/N_B equilibrium ratio has been frozen in, considering our experimental cooling rates and the measured $B \rightarrow A$ conversion rates, Fig. 20(b).

The ratio of N_A/N_B was estimated from Fig. 19 for each of the B-, Al-, and Ga-doped samples. In Eq. (11) we take $\Delta E_{AB}^0 = 0.017$ eV and $\Delta E_A = 0.09$ eV, as determined in Sec. IV D. ΔE_B therefore is the only unknown, which we have solved for graphically in Fig. 21 by comparing the experiment estimates of N_A/N_B versus μ with Eq. (11). The best estimated value for ΔE_B is 0.050 ± 0.005 eV. We have now been able to determine all of the relevant energies and barriers for each of the three charge states of the bistable $C_i C_s$ defects.

The value ~ 0.05 eV for the emission energy of the B^+ charge state is reasonable. It explains why we were not able to detect it with DLTS because it is too shallow. The failure to detect the B^+ configuration by EPR may also result from its shallow character. Shallow acceptors, for example, are very difficult to detect because they are strongly inhomogeneously broadened due to internal random strains.^{60,61}

V. MODEL AND DISCUSSION

A. Configurational-coordinate diagram

Figure 22 gives a complete configurational-coordinate diagram of the $C_i C_s$ pair. We have determined all of the

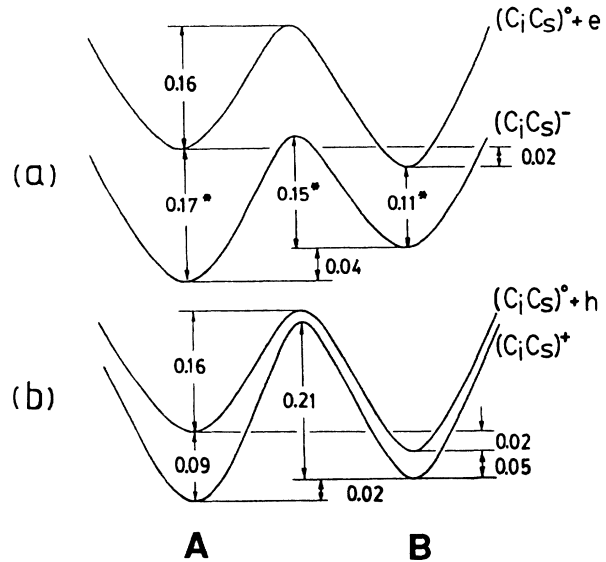


FIG. 22. Final configurational-coordinate energy diagram for the $C_i C_s$ pair (units in eV). (a) The acceptor state; (b) the donor state. [The asterisked values are those determined by Jellison (Ref. 13).]

relevant energy values in addition to those originally obtained by Jellison¹³ for the $E_c - 0.17$ eV bistable defect. The hole emission activation energy for A^+ is 0.09 eV which is smaller than the thermal barrier for the $A^0 \rightarrow B^0$ conversion. As a result, we have been able to determine the $A^0 \rightarrow B^0$ barrier in the p -type studies. From Fig. 22(a) we notice that one could not have measured this barrier in the n -type studies simply because the $A^- \rightarrow A^0 + e^-$ emission has a higher barrier than the $A^0 \rightarrow B^0$ conversion. That explains why the $A^- \rightarrow B^0$ conversion rate measured by Jellison was identical to the $A^- \rightarrow A^0 + e^-$ emission rate.¹³

The configurational-coordinate diagrams we have drawn do not show lattice relaxation. No shift in the configurational coordinate at each energy minimum has been indicated when the defect changes its charge state. This is probably correct for the B configuration since a strong zero-phonon-optical transition at 0.97 eV associated with the B^0 configuration has been observed in both absorption and emission.²⁶⁻²⁸ For the A configuration, however, no experimental information is available to distinguish whether or not significant lattice relaxation is involved. This probably could only be answered by using an optically assisted technique, e.g., optical DLTS.⁶⁵

B. Structural model

The microscopic model that we propose for the A configuration is shown in Fig. 23. This model, which is different from that proposed originally by Brower for Si-G11,⁴⁶ is developed as follows: (1) For both $(C_i C_s)^-$ and $(C_i C_s)^+$ the “dumbbell” $\text{Si}_i\text{-C}_i$ interstitialcy character of isolated C_i (Ref. 41) is retained. The evidence for this is

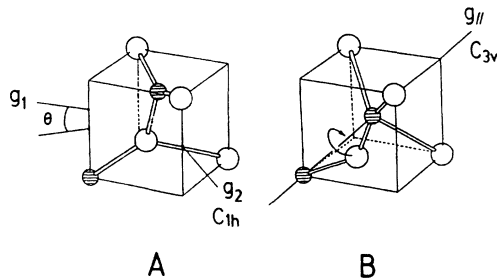


FIG. 23. Models for the two configurations of the $C_i C_s$ pair. The smaller cross-hatched atoms are carbon.

the close similarity in magnitude and sense of the restricted $\langle 100 \rangle$ stress-induced alignment for Si-G11 ($C_i C_s$)⁺ and Si-G17 ($C_i C_s$)⁻ to that for isolated C_i monitored by Si-G12 (C_i)⁺ and Si-L6 (C_i)⁻. (2) The very similar ^{13}C hyperfine interaction for the β carbon in ($C_i C_s$)⁺ compared with that for C_i ⁺ indicates that the C_β -Si interstitialcy character remains in the donor state of $C_i C_s$ as well. (3) Therefore, the *A* configuration is basically an isolated carbon-silicon interstitialcy (C_i) but slightly perturbed by the presence of a second carbon atom. The second carbon atom is in the substitutional site shown in Fig. 23(a) where it serves to reduce the compressive strain along the Si-Si-Si chain because of its smaller size. (4) The easy conversion from the *A* to *B* configuration, as will be discussed next, is also easily understood with this model. Therefore the model for the *A* configuration has one substitutional carbon atom next to a C—Si interstitialcy in which a carbon-silicon “molecule” shares a single lattice site, each component being threefold coordinated.

We have demonstrated that the 0.97-eV luminescence arises also from the same $C_i C_s$ bistable defect and from the *B* configuration only. This is also confirmed by the close similarity of the B^- (Si-L7) EPR spectrum and the ODMR spectrum of the luminescence.⁴⁸ As discussed earlier, the EPR spectrum shows a motional averaging feature with C_{3v} symmetry at $T \geq 15$ K, but reduced symmetry at lower temperature. This is similar to the observation in the ODMR studies, where the $S = 1$ ODMR spectrum motionally averages from C_{1h} ($T \sim 1.7$ K) to C_{3v} ($T \sim 30$ K) along a particular $\langle 111 \rangle$ axis.⁴⁸ In the motionally averaged state, both display the unusual satellite structure shown in Fig. 5(a) and Ref. 48. This structure matches well that predicted for equal ^{29}Si hyperfine coupling ($A^{29} = 7.5 \times 10^{-4} \text{ cm}^{-1}$ for the Si-L7 center and $A^{29} = 4.7 \times 10^{-4} \text{ cm}^{-1}$ for the ODMR spectrum) with ~ 24 silicon neighbors. In the ODMR studies, additional hyperfine interactions with two equivalent carbon atoms and one single silicon atom led to a model of two substitutional carbon atoms with the silicon atom squeezed between in a position slightly off the bond center.⁴⁸ We therefore assign this structure to the *B* configuration, as illustrated in Fig. 23(b). This model is fully consistent with the B^- (Si-L7) EPR signal if we assume that the paramagnetic electron is spread primarily over a cage of

~ 24 silicon atoms. It is also consistent with the excited $S = 1$ B^0 state observed by ODMR in the luminescence, if the electron is similarly distributed and the accompanying hole is localized primarily on the C_s -Si_i- C_s core. The observation that the A^{29} tensor for the ODMR spectrum is roughly one-half as large as for the Si-L7 center lends credence to this model. The excited $S = 1$ ODMR state is a two-spin system with a moderate size spin-spin interaction (fine-structure *D* term). For such a system, the hyperfine interaction at any site should be the average of the hyperfine interactions with the two $S = \frac{1}{2}$ particles.⁴⁸ For spatially separated particles as suggested above, this predicts approximately one-half the hyperfine interaction for the ^{29}Si cage as that seen for the $S = \frac{1}{2}$ electron alone in Si-L7. This is what is observed. The hyperfine interaction in the ODMR state is a little more than half of that for the Si-L7 center, indicating some overlap between the electron and hole components. We conclude, therefore, that in the *B* configuration, two substitutional carbon atoms (each fourfold coordinated) are in normal lattice sites with a twofold coordinated silicon atom squeezed off-center between them. The intraconversion between the *A* and *B* configuration requires only a simple switching of bonds.

C. Mechanism for bistability

The mechanism for the bistability clearly comes from a molecular bond switching between two configurations that are very close in energy. That they are energetically comparable makes sense in that in each configuration there are the same number of bonds and therefore the same number of unbonded orbitals on the atoms which supply the states in the gap. On the other hand, it is most surprising that the energy differences are as small as they are (~ 0.02 eV) in each of the three charge states. Apparently the effect of the small but real chemical difference between carbon and silicon is accidentally compensated by the effect of their size differences to make these two configurations so close in energy. It should be a real challenge to a theorist to duplicate these results and provide a good physical picture for the driving forces and the effect of charge state.

It is interesting to note that the reorientation kinetics observed by EPR for ($C_i C_s$)⁺ and ($C_i C_s$)⁻, Fig. 11, give a barrier of ~ 0.2 eV, close to that for the *A* \rightarrow *B* conversion as deduced from the bistability studies and summarized in Fig. 22. This suggests that reorientation from one *A* configuration to another goes by way of bond switching to the *B* configuration which according to our models of Fig. 23 is symmetrically disposed with respect to the three possible orientations of the Si—C interstitialcy around the substitutional carbon. This supplies an important additional confirmation of our models.

D. Local-mode structure

We have shown that the 0.97-eV luminescence arises from the *B* configuration only. Superficially, this interpretation appears in conflict, however, with evidence from resolved carbon local-mode structure on the 0.97-eV

luminescence band. Optical studies^{28,66} in isotopically ^{13}C -enriched samples have identified a sharp phonon sideband feature in both absorption and luminescence as a vibrational local mode which involves a *single* carbon atom. After ODMR studies^{47,48} showed that two equivalent carbon atoms are involved in the 0.97-eV luminescence, more careful studies on this local mode structure were made and showed that there is some evidence of a perturbation from a second carbon atom.^{67,68} The ^{12}C local mode in a ^{13}C -doped sample (60% ^{13}C -40% ^{12}C) was found to be shifted to lower energy by ~ 0.08 meV, and broadened as shown in Fig. 24(a). It was confirmed therefore that the 0.97-eV optical center involves two carbon atoms but it was concluded that they are *inequivalent*.⁶⁷ The *A* configuration fits that interpretation better, lending support at the time to a previous suggestion that the *B* configuration may be only indirectly involved in the luminescence pumping cycle.⁴⁸ We have now concluded, however, that the 0.97-eV luminescence arises from the *B* configuration. In order to explain this, we will now explore an alternative interpretation—that the local-mode structure results from a very weakly coupled interaction between vibrational modes of the two

carbon atoms in the *B* configuration.

One phonon local-mode sidebands are strictly forbidden in an electronic transition unless they transform as the completely symmetric (A_1) representation of the defect group symmetry.⁶⁹ An isolated bent C-Si-C molecule has C_{2v} symmetry and only the symmetric modes of the two equivalent carbon atoms in the plane of the molecule are, therefore, allowed. Embedded in the silicon lattice, Fig. 23 (*B*), the symmetry is actually lowered to C_{1h} . Vibrations perpendicular to the C_{1h} plane remain forbidden, but classification of the in-plane vibrations as symmetric or antisymmetric is no longer strictly valid. However, the departure from C_{2v} symmetry comes only from second neighbors and the classification of the in-plane modes by their symmetry in C_{2v} remains instructive. The effect of a small reduction in symmetry should primarily be only to destroy the exact equivalence of the two carbons making the “antisymmetric” mode (now more one of the carbons than the other) weakly allowed.

Consider therefore that the in-plane vibrations of the two carbon atoms (equivalent in C_{2v}) are coupled only very weakly. For the defects containing two ^{12}C atoms or two ^{13}C atoms, this coupling causes the symmetric and antisymmetric mode frequencies to be split by 2δ around each of the uncoupled ^{12}C and ^{13}C vibrational frequencies (separated by the isotope shift $\Delta \gg \delta$) as shown in Fig. 24(b). The allowed symmetric modes are indicated as solid lines in the figure with the antisymmetric modes shown dashed. For a ^{12}C - ^{13}C defect, the off-diagonal coupling produces only a negligible effect and the two vibrational modes are just the uncoupled vibrational modes of each as shown also in Fig. 24(b). In the figure, the vertical heights of the solid lines represent the expected intensities predicted for the 40% ^{12}C -60% ^{13}C isotope ratio in our sample. Comparison with the experimental observations in (a) gives a very good fit to the observed line positions and shapes with $\delta \sim 0.08$ meV.

To investigate whether such a small coupling is physically reasonable, we have constructed a simple model of the defect using appropriate masses and a single force-constant spring between each carbon atom and its neighbors (the central silicon atom plus the three lattice silicon atoms to which it is bonded). The silicon neighbors were held fixed and the in-plane normal mode frequencies for the C-Si-C molecule were calculated as a function of the angle α between the two carbon bonds to the central silicon atom. Such a model leads to strong coupling between the two carbon atoms except in the vicinity of $\alpha = 90^\circ$, where the coupling goes to zero and the symmetric and anti-symmetric high frequency (local) modes cross. If weaker bond bending forces are added at the central silicon, the angle for decoupling changes ($\alpha > 90^\circ$) but it always occurs.

Such a treatment is not quantitative, of course. We have no direct independent information about the C—Si bond bending and stretching spring constants, nor of the angle α . However, we conclude that this model can supply a reasonable explanation for the local mode structure. If correct, the bond angle α must be close to 90° , providing us in turn with our first estimate of how far the Si atom may be displaced off bond center, an important mi-

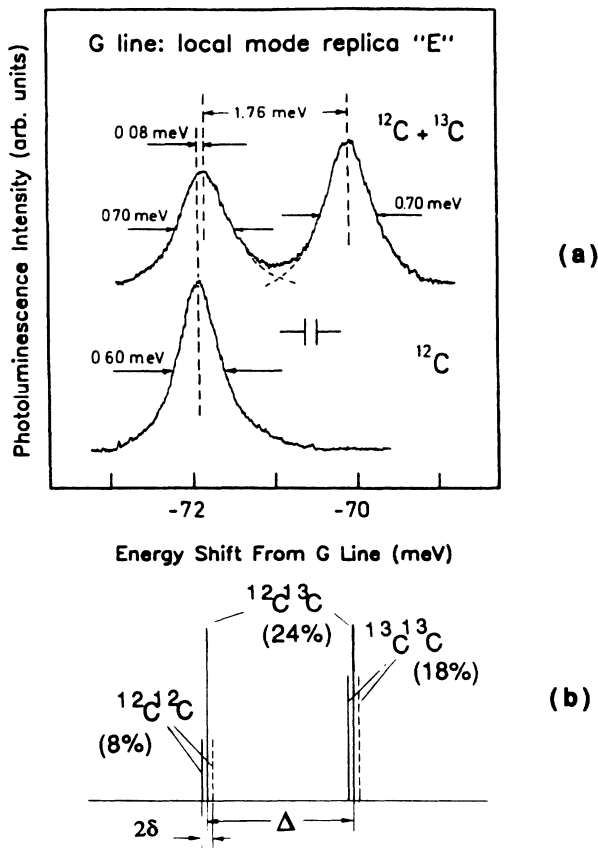


FIG. 24. (a) One-phonon local-mode replicas of the 0.97-eV luminescence indicating the shift and broadening of the ^{12}C mode in a ^{13}C -enriched (60%) sample (taken from Ref. 68). (b) The replica structure predicted for weakly coupled modes of two equivalent carbon atoms in the ^{12}C (40%)– ^{13}C (60%) sample.

croscopic feature of interest.

It is important to note that the model for the B configuration of Fig. 23 was deduced from ODMR studies of an excited $S=1$ state directly involved in the luminescence pumping cycle but not the excited state associated with the luminescence or absorption transition. (No Zeeman splitting has been detected, which indicates $S=0$ in the initial and final states of the optical transition.²⁸) For this $S=1$ state, the two carbon atoms were observed to be closely equivalent and the off-center silicon atom was observed to undergo rapid motion around the C—C bond axis at $T > 20$ K. This suggests that for this state, the silicon atom may be only slightly off bond center, $\alpha > 90^\circ$. The local-mode structure, however, reflects the properties of the ground and excited $S=0$ states for which our simple analysis suggests a large off-axis displacement of the Si atom, with $\alpha \sim 90^\circ$. Such a singlet-triplet relaxational change is not unreasonable and might explain the failure to see evidence of this rotational motion in the optical absorption and luminescence versus temperature, as recently reported.⁷⁰

E. Energy-level positions

The energy-level position for the C_iC_s acceptor state was estimated from the EPR studies in Sec. IV B to be in the region of $E_c - 0.045 \text{ eV} < E_t < E_c - 0.17 \text{ eV}$. On the other hand, the thermal emission rate measured by DLTS indicated a level at $E_c - 0.17 \text{ eV}$. From the configurational-coordinate diagram, Fig. 22, we can now understand the origin of this discrepancy. The definition of a defect energy-level position with respect to the conduction- (or valence-) band edge is the total energy difference between the lowest energy state when the trap is filled and the lowest energy state when the trap is empty, with the electron (or hole) in the conduction (or valence) band. In the case of the C_iC_s acceptor state, the energy-level position is given therefore by the energy difference between A^- and $B^0 + e^-$. This value is less than the emission activation energy from A^- to A^0 , which is what is measured by DLTS. From Fig. 22, we find the true level position to be $E_c - 0.15 \text{ eV}$, which agrees well with the EPR result. The same argument ap-

plies to the donor state of C_iC_s . Its true energy-level position should be at $E_v + 0.07 \text{ eV}$.

In general, one should therefore be cautious when dealing with a metastable system. After thermal emission, the defect will not always end up in the lowest energy configuration of the upper state. The true level position is best determined by measuring occupancy under thermodynamic equilibrium with the Fermi level, as in the EPR experiment (or in a Hall measurement).

F. Wave-function distribution

The weak ^{13}C hyperfine interactions indicate that the spin wave function is localized only weakly on the carbon atoms when the C_iC_s pair is in its negatively charged state. No resolvable ^{13}C hyperfine interaction can be detected at all for the B^- configuration (Si-L7). These observations are consistent with the models we have proposed. In the A configuration, the core structure of the C_iC_s pair is essentially that of the isolated C_i defect, only slightly perturbed by the second C_s atom. In the preceding paper³⁶ we have shown that ^{13}C hyperfine interactions are undetectable for C_i^- and we have presented a simple molecular orbital model of the defect which explains why the unpaired spin does not localize on the carbon atom. Therefore, the same situation is applicable to $(C_iC_s)^-$ because of the dominant C_i^- character of the wave function. The failure to detect a single ^{29}Si hyperfine interaction suggests that the wave function may be spread instead over many neighbors. In the B^- configuration, ^{29}Si hyperfine interaction in its motionally averaged state shows that the spin wave function is spread over ~ 24 silicon neighboring sites. This plus the complete absence of resolved ^{13}C interactions suggests that the spin wave function may be even more delocalized in the B^- configuration. These suggestions could be tested if one could employ the ENDOR technique in the study.

ACKNOWLEDGMENTS

This work was supported by the United State Office of Naval Research Contract No. N00014-84-K-0025 and National Science Foundation Grant No. DMR-85-20269.

*Present address: Department of Physics and New York State Institute on Superconductivity, State University of New York at Buffalo, Amherst, NY 14260.

¹G. D. Watkins, *Mater. Sci. Forum* **38-41**, 39 (1989).

²A. Chantre, in *Defects in Electronic Materials*, Vol. 104 of *The Materials Research Proceedings*, edited by M. Stavola, S. J. Pearton, and G. Davies (MPS, Pittsburgh, 1988), p. 37.

³D. V. Lang, in *Deep Centers in Semiconductors*, edited by S. Pantelides (Gordon and Breach, New York, 1986), Chap. 7.

⁴G. M. Martin and S. Markram-Ebeid, in Ref. 3, Chap. 6.

⁵J. E. Dmochowski, J. M. Langer, and Z. Kalinski, *Phys. Rev. Lett.* **56**, 1735 (1986).

⁶L. F. Makarenko, V. P. Markevich, and L. I. Murin, *Fiz. Tekh. Poluprovodn.* **19**, 1935 (1985) [*Sov. Phys.—Semicond.* **19**, 1192 (1985)].

⁷P. Wagner and J. Hage, *Appl. Phys. A* **49**, 123 (1989).

⁸V. V. Litvinov, G. V. Palchik, and V. I. Urenev, *Phys. Status Solidi A* **108**, 311 (1988).

⁹M. Stavola, M. Levinson, J. L. Benton, and L. C. Kimerling, *Phys. Rev. B* **30**, 832 (1984).

¹⁰M. Levinson, M. Stavola, P. Besomi, and W. A. Bonner, *Phys. Rev. B* **30**, 5817 (1984).

¹¹A. Chantre and D. Bois, *Phys. Rev. B* **31**, 7979 (1985).

¹²A. Chantre and L. C. Kimerling, *Mater. Sci. Forum* **10-12**, 387 (1986).

¹³G. E. Jellison, Jr., *J. Appl. Phys.* **53**, 5715 (1982).

¹⁴J. L. Benton and M. Levinson, in *Defects in Semiconductors II*, edited by S. Mahajan and J. W. Corbett (North-Holland, New York, 1983), p. 95.

¹⁵L. W. Song, B. W. Benson, and G. D. Watkins, *Phys. Rev. B*

- 33, 1452 (1986).
- ¹⁶A. Chantre and L. C. Kimerling, *Appl. Phys. Lett.* **48**, 1000 (1986).
- ¹⁷M. T. Asom, J. L. Benton, R. Sauer, and L. C. Kimerling, *Appl. Phys. Lett.* **51**, 256 (1987).
- ¹⁸L. W. Song, B. W. Benson, and G. D. Watkins, *Appl. Phys. Lett.* **51**, 1155 (1987).
- ¹⁹L. W. Song, X. D. Zhan, B. W. Benson, and G. D. Watkins, *Phys. Rev. Lett.* **60**, 460 (1988).
- ²⁰L. W. Song, X. D. Zhan, B. W. Benson, and G. D. Watkins, in *Defects in Electronic Materials*, Vol. 104 of *Materials Research Society Symposia Proceedings*, edited by M. Stavola, S. J. Pearton, and G. Davies (MRS, Pittsburgh, 1988), p. 79.
- ²¹S. K. Bains and P. C. Banbury, *J. Phys. C* **18**, L109 (1985).
- ²²A. Chantre, *Phys. Rev. B* **32**, 3687 (1985).
- ²³O. O. Awadelkarim and B. Monemar, *Phys. Rev. B* **38**, 10116 (1988).
- ²⁴J. H. Svensson and B. Monemar, *Phys. Rev. B* **40**, 1410 (1989).
- ²⁵B. W. Benson, E. Gurer, and G. D. Watkins, *Mater. Sci. Forum* **38-41**, 391 (1989).
- ²⁶A. V. Yukhnevitch and A. V. Mudryi, *Fiz. Tekh. Poluprovodn.* **7**, 1215 (1977) [*Sov. Phys.—Semicond.* **7**, 815 (1973)].
- ²⁷C. P. Foy, M. C. do Carmo, G. Davies, and E. C. Lightowers, *J. Phys. C* **14**, L7 (1981).
- ²⁸K. Thonke, H. Klemisch, J. Weber, and R. Sauer, *Phys. Rev. B* **24**, 5874 (1981).
- ²⁹R. C. Newman and J. B. Willis, *J. Phys. Chem. Solids* **26**, 373 (1965).
- ³⁰Annual Book of ASTM Standards, Vol. 10.05 (ASTM, Philadelphia, 1988).
- ³¹W. Kaiser, P. H. Keck, and C. F. Lange, *Phys. Rev.* **101**, 1264 (1956).
- ³²G. D. Watkins and J. W. Corbett, *Phys. Rev.* **121**, 1001 (1961).
- ³³J. W. Corbett, G. D. Watkins, R. M. Chrenko, and R. S. McDonald, *Phys. Rev.* **121**, 1015 (1961).
- ³⁴D. V. Lang, *J. Appl. Phys.* **45**, 3023 (1974).
- ³⁵G. L. Miller, D. V. Lang, and L. C. Kimerling, *Annu. Rev. Mater. Sci.* **7**, 377 (1977).
- ³⁶L. W. Song and G. D. Watkins, preceding paper, *Phys. Rev. B* **42**, 5759 (1990).
- ³⁷J. W. Corbett, G. D. Watkins, and R. S. McDonald, *Phys. Rev.* **135**, A1381 (1964).
- ³⁸A. R. Bean and R. C. Newman, *Solid State Commun.* **8**, 175 (1970).
- ³⁹J. M. Trombetta and G. D. Watkins, *Appl. Phys. Lett.* **51**, 1103 (1987).
- ⁴⁰G. D. Watkins, in *Lattice Defects in Semiconductors, 1974*, IOP Conf. Proc. Ser. No. 23, edited by F. A. Huntley (IOP, Bristol, 1975), p. 1.
- ⁴¹G. D. Watkins and K. L. Brower, *Phys. Rev. Lett.* **36**, 1329 (1976).
- ⁴²L. C. Kimerling, in *Radiation Effects in Semiconductors, 1976*, IOP Conf. Proc. Ser. No. 31, edited by N. B. Urli and J. W. Corbett (IOP, London, 1977), p. 221.
- ⁴³P. M. Mooney, L. J. Cheng, M. Suli, J. D. Gerson, and J. W. Corbett, *Phys. Rev. B* **15**, 3836 (1977).
- ⁴⁴R. Woolley, E. C. Lightowers, A. K. Tipping, M. Claybourn, and R. C. Newman, *Mater. Sci. Forum* **10-12**, 929 (1986).
- ⁴⁵K. Thonke, A. Teschner, and R. Sauer, *Solid State Commun.* **61**, 24 (1987).
- ⁴⁶K. L. Brower, *Phys. Rev. B* **9**, 2607 (1974).
- ⁴⁷K. M. Lee, K. P. O'Donnell, J. Weber, B. C. Cavenett, and G. D. Watkins, *Phys. Rev. Lett.* **48**, 37 (1982).
- ⁴⁸K. P. O'Donnell, K. M. Lee, and G. D. Watkins, *Physica B+C (Amsterdam)* **116B**, 258 (1983).
- ⁴⁹G. Davies, A. Oates, R. C. Newman, R. Woolley, E. C. Lightowers, M. Binns, and J. Wilkes, *J. Phys. C* **19**, 841 (1986).
- ⁵⁰A. V. Yukhnevich and V. D. Tkachev, *Fiz. Tverd. Tela (Leningrad)* **8**, 1264 (1966) [*Sov. Phys.—Solid State* **8**, 1004 (1966)].
- ⁵¹G. D. Watkins, in *Radiation Damage in Semiconductors* (Dunod, Paris, 1964), p. 97.
- ⁵²L. C. Kimerling, P. Blood, and W. M. Gibson, in *Defects and Radiation Effects in Semiconductors, 1978*, edited by J. H. Albany, IOP Conf. Ser. No. 46 (IOP, London, 1979), p. 273.
- ⁵³R. D. Harris and G. D. Watkins, in *The 13th International Conference on Defects in Semiconductors*, edited by L. C. Kimerling and J. M. Parsey, Jr. (AIME, New York, 1985), p. 799.
- ⁵⁴L. C. Kimerling, M. T. Asom, J. L. Benton, P. J. Drevinsky, and C. E. Cafer, *Mater. Sci. Forum* **38-41**, 141 (1989).
- ⁵⁵A. M. Portis, Sarah Mellon Scaife Radiation Laboratory Report 1955 (unpublished).
- ⁵⁶G. D. Watkins and J. W. Corbett, *Phys. Rev.* **134**, A1359 (1964).
- ⁵⁷G. D. Watkins and J. W. Corbett, *Phys. Rev.* **138**, A543 (1965).
- ⁵⁸L. J. Cheng, J. C. Corelli, J. W. Corbett, and G. D. Watkins, *Phys. Rev.* **152**, 761 (1966).
- ⁵⁹H. Y. Fan and A. K. Ramdas, *J. Appl. Phys.* **30**, 1127 (1959).
- ⁶⁰G. Feher, J. C. Hensel, and E. A. Gere, *Phys. Rev. Lett.* **5**, 309 (1960).
- ⁶¹W. Kohn, in *Solid State Physics*, edited by F. Seitz and D. Turnbull (Academic, New York, 1957), Vol. 5, p. 257.
- ⁶²J. I. Pankove, *Optical Processes in Semiconductors* (Prentice-Hall, Englewood Cliffs, NJ, 1971).
- ⁶³A. K. Ramdas and S. Rodriguez, *Rep. Prog. Phys.* **44**, 1297 (1981).
- ⁶⁴J. S. Blakemore, *Semiconductor Statistics* (Pergamon, New York, 1962).
- ⁶⁵M. Stavola, M. Levinson, J. L. Benton, and L. C. Kimerling, *Phys. Rev. B* **30**, 832 (1984).
- ⁶⁶G. Davies and M. C. do Carmo, *J. Phys. C* **14**, L687 (1981).
- ⁶⁷G. Davies, E. C. Lightowers, and M. C. do Carmo, *J. Phys. C* **16**, 5503 (1983).
- ⁶⁸K. Thonke, Ph.D. thesis, University of Stuttgart, 1986 (unpublished).
- ⁶⁹G. Herzberg, *Molecular Spectra and Molecular Structure*, 2nd ed. (Van Nostrand, New York, 1950).
- ⁷⁰G. Davies, H. Brian, E. C. Lightowers, K. Barraclough, and M. F. Thomaz, *Semicond. Sci. Technol.* **4**, 200 (1989).